Origin of the Nizhny Tagil Clinopyroxenite–Dunite Massif, Uralian Platinum Belt, Russia: Insights from PGE and Os Isotope Systematics

Svetlana G Tessalina, Kreshimir N Malitch, Thierry Augé, Victor N Puchkov, Elena Belousova, Brent I A Mcinnes

JOURNAL OF PETROLOGY

Journal of Petrology, 2016, Vol. 56, No. 12, 2297–2318
doi: 10.1093/petrology/egv077
Advance Access Publication Date: 14 January 2016
Original Article

OXFORD

Origin of the Nizhny Tagil Clinopyroxenite–Dunite Massif, Uralian Platinum Belt, Russia: Insights from PGE and Os Isotope Systematics

Svetlana G. Tessalina[1,*], Kreshimir N. Malitch[2], Thierry Augé[3], Victor N. Puchkov[4], Elena Belousova[5] and Brent I. A. McInnes[1]

[1]John de Laeter Centre for Isotope Research & The Institute for Geoscience Research (TIGeR), Faculty of Science and Engineering, Curtin University, Kent Street, Bentley, WA 6102, Australia; [2]Institute of Geology and Geochemistry, Ural Branch of Russian Academy of Sciences, Pochtovy 7, 620075, Ekaterinburg, Russia; [3]BRGM, Georesources Division, 3, Av. Claude-Guillemin, BP36009, 45060 Orléans cedex 2, France; [4]Institute of Geology, Ufimian Scientific Centre of Russian Academy of Sciences, K.Marx st., 16/2, 450 000 Ufa, Russia; Bashkirian State University, Russia and [5]ARC Centre of Excellence for Core to Crust Fluid Systems (CCFS) and GEMOC National Key Centre, Department of Earth and Planetary Sciences, Macquarie University, Sydney, NSW 2109, Australia

*Corresponding author. E-mail: Svetlana.Tessalina@curtin.edu.au

Received November 5, 2014; Accepted December 2, 2015

ABSTRACT

Zoned clinopyroxenite–dunite Uralian–Alaskan-type complexes of the Uralian Platinum Belt are the source of economic platinum deposits. One of the striking features of Uralian–Alaskan-type complexes is a pronounced Pt anomaly, which clearly distinguishes them from cumulate series of ophiolite massifs elsewhere, but there is still uncertainty regarding the nature of the platinum enrichment and its geodynamic setting. We have studied the platinum-group element (PGE) and Os isotope systematics of platinum-group minerals, chromitites and ultramafic rocks from the Nizhny Tagil zoned clinopyroxenite–dunite massif in the Urals. The whole-rock $^{187}Os/^{188}Os$ ratios of the dunites vary from 0·1160 to 0·1332, averaging 0·1247, with more radiogenic values possibly affected by subduction-related fluids during Tagil island arc development (*c.* 410 Ma). Laurite and Os–Ir alloys have $^{187}Os/^{188}Os$ ratios of $0{\cdot}12245 \pm 0{\cdot}00038$, which are close to those of chromitites ($^{187}Os/^{188}Os = 0{\cdot}1215 \pm 0{\cdot}0006$) and correspond to an Os model age (T_{RD}) of *c.* 800 Ma. This model age is *c.* 400 Myr older than a melt depletion event corresponding to Tagil island arc development, and can be ascribed to a Neoproterozoic mantle melting event under the influence of either a pre-Uralian subduction zone or a superplume, overprinted by younger processes. The Pt/Pd values in the ultramafic rocks show significant variations, increasing towards the chromite-PGE-bearing mineralization zone. The overall primitive mantle normalized PGE patterns are very similar to those reported for sub-arc mantle peridotites, which are characterized by a positive slope and high Pt/Pd ratios, and are distinct from those of typical peridotites and cumulates from Urals ophiolite massifs. Such a similarity may be explained by the melting of metasomatized depleted mantle that had undergone several melt extraction events in a subduction-zone setting. This is also evident from a high oxygen fugacity averaging 2·7 relative to fayalite–magnetite–quartz, which is distinctly more oxidized compared with mid-ocean ridge basalt and ocean island basalt settings. However, the striking similarities (P–T–fO_2 and type of parental magma, high Pt/Pd ratio) to other zoned clinopyroxenite–dunite massifs such as Kondyor, situated within the stable Archean shield, allow us to conclude that this type of massif is not exclusive to subduction-zone settings, but may reflect the presence of a specific depleted, fluid-metasomatized type of relatively shallow mantle in the Paleozoic. The systematic Pt/Pd ratio increase in the Nizhny Tagil rocks towards the chromite mineralized zone suggests that Pt–Pd fractionation may be related to the preferential retention of Pt in chromitites as Pt–Fe alloys.

Key words: Nizhny Tagil; Urals; Uralian–Alaskan type; peridotite; platinum-group elements; Os isotopes

INTRODUCTION

Uralian–Alaskan-type complexes were originally defined by Taylor (1967) as mantle-derived, concentrically zoned, olivine-rich intrusions evolving from a dunite-rich core to a clinopyroxenite-rich rim, with gabbro or diorite at the margins. The distinctive feature of Uralian–Alaskan-type complexes compared with other ultramafic bodies is the virtual absence of orthopyroxene. There are approximately 46 known clinopyroxenite–dunite massifs worldwide (Guillou-Frottier *et al.*, 2014) that fit the above definition of a Uralian–Alaskan-type ultramafic complex. They are economically significant, particularly in the Uralian Platinum Belt (UPB), where the mining of platinum-group minerals (PGM) and Pt–Fe alloys represents the second largest source of Russian platinum after the Noril'sk-type Cu–Ni sulfide ores (Foley *et al.*, 1997; Garuti *et al.*, 1997). Previous workers have interpreted Uralian–Alaskan-type ultramafic massifs as (1) cumulate igneous rocks formed in a magma chamber that crystallized from a depleted mantle-derived magma in a suprasubduction-zone environment (Borg & Hattori, 1997; Ivanov, 1997), (2) residual mantle tectonites emplaced in the lithosphere (Maegov *et al.*, 2006) and (3) deep-seated cumulates diapirically emplaced at a high level in the crust (e.g. Fershtater, 2013).

One of the distinguishing features of Uralian–Alaskan-type complexes is their anomalous Pt concentrations compared with ultramafic rocks from ophiolite complexes (cumulate series) and other tectonic settings (Garuti *et al.*, 1997). The Pt anomaly has been interpreted as a distinctive feature of a primitive subalkaline picritic basalt magma derived from a sub-arc mantle wedge source (Garuti *et al.*, 1997), as evidenced by a recent study of melt inclusions in Cr-spinel from the Nizhny Tagil massif (Simonov *et al.*, 2013). However, the close similarity of the Nizhny Tagil massif to stable craton hosted Alaskan-type (so-called Aldan-type) dunite–clinopyroxenite massifs such as Kondyor make this geodynamic interpretation questionable. Moreover, the interpretation of the UPB dunite–clinopyroxenite–gabbro complexes as suprasubduction-zone related rocks is complicated by new geochronological data (e.g. Ronkin *et al.*, 1997, 2009, 2012; Maegov *et al.*, 2006; Popov & Belyatsky, 2006; Efimov, 2010; Petrov *et al.*, 2010) for UPB rocks that yield ages pre-dating Urals island arc formation (mostly Late Neoproterozoic Sm–Nd ages), and ancient U–Pb ages of zircons extracted from dunites, ranging from Neoarchean to Mid-Paleozoic (Fershtater *et al.*, 2009; Malitch *et al.*, 2009). This new geochronological dataset reflects the multi-stage formation history of the Uralian Platinum Belt.

In this work we investigate platinum-group minerals, chromitites and ultramafic rocks from the Nizhny Tagil massif using trace element, platinum-group element (PGE) and Re–Os isotope analysis techniques, along with previously published and new data on the P–T–fO_2 conditions of its formation, to better understand its petrogenesis.

GEOLOGICAL SETTING AND SAMPLING

Geological setting

The Nizhny Tagil massif is located 50 km SW of the city of Nizhny Tagil in the southern part of the ~1000 km long Uralian Platinum Belt (Fig. 1). The massif is fault-bounded to the west where it is juxtaposed against a package of Ordovician–Silurian volcano-sedimentary rocks of island arc affinity (Shmelev & Sedler, 1999; Shmelev, 2007), whereas to the east the outer massif

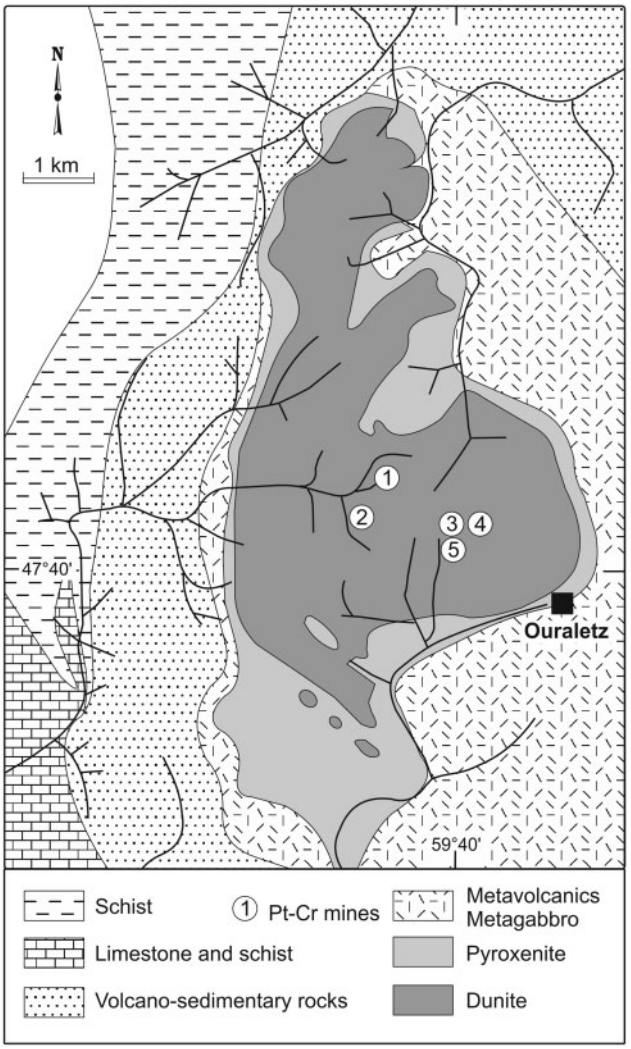

Fig. 1. Geological sketch map of the Nizhny Tagil massif [adapted from Augé *et al.* (2005)] showing the location of quarries: 1, Goshachta; 2, Krutoy Log; 3, Alexandrovsky; 4, Sirkov Log; 5, Solovyovogorsk. Lines represent drainage systems.

borders migmatized amphibolites and pyroxene–amphibole banded hornfels (so called kytlymites) with interbedded metasedimentary rocks of unknown age. These rocks are gradually replaced to the east by gneissic and schistose banded amphibolites. Based on their relatively low Ti contents and enrichment in large-ion lithophile elements (LILE), the metamorphic mafic rocks to the east are also thought to be subduction-related (Shmelev & Sedler, 1999; Shmelev, 2007).

The Nizhny Tagil massif covers a total area of ~47 km^2 with a central dunite core of ~28 km^2 (Fig. 1). It is largest of the 10 known dunite bodies of the Uralian Platinum Belt in terms of area. Geophysical data suggest that its structure can be traced to a depth of 10–15 km, after which it gradually flattens and tapers out (Sokolov, 1989).

The dunite core is surrounded by a continuous rim of olivine-bearing clinopyroxenite, which varies in thickness from 100 m to 2000 m in the southwestern part of the massif. Locally a narrow rim of wehrlite separates the dunite and pyroxenite units. The external contact of the clinopyroxenite with the host-rocks is relatively sharp, whereas the internal contact with the dunite is undulating. In addition, several lenticular bodies of clinopyroxenite (with a length of up to 0·5–1·5 km) have been observed to occur within the dunite itself. Platinum mineralization is associated with chromite segregations, schlieren and veins formed late in the magmatic evolution of the massif. Where they occur in economic concentrations in hard rock they are referred to as Nizhny Tagil late-magmatic platinum deposits (Ivanov, 1997). Platinum-group minerals and alloys are also mined in placer deposits near and within the massif.

Zircons extracted from the dunites of the Nizhny Tagil massif show a wide range of U–Pb ages from Neoarchean (2781 ± 56 Ma), Paleoproterozoic (2487 ± 33 and 1881 ± 9 Ma) and Mesoproterozoic (1172 ± 10 Ma) to Mid-Paleozoic (414·8 ± 3·9 and 473 ± 3·7 Ma) (Fershtater *et al.*, 2009; Malitch *et al.*, 2009).

Sampling strategy

We have studied a suite of eight dunite samples across a zone of primary mineralization, one sample of the pyroxenite rimming the dunite core and two samples of massive chromitite (Fig. 2).

Dunites (samples 2VA, 6VA, 8VA, 9VA, 10VA, 11VA, 16VA and NT10) have an adcumulate texture. Olivine is extensively replaced by serpentine, with the degree of serpentinization varying from 40 to 60%. Chromite in the dunite (1–5 vol. %) exhibits a large variety of habits, ranging from very small (10 μm) euhedral grains to large subrounded crystals. The chromite systematically shows secondary cracks that are attributed to volume changes during serpentinization. Rare interstitial clinopyroxene has been observed in some of the dunites, but orthopyroxene is characteristically absent.

The chromite-bearing facies have various textures, the most common being thin (up to 5 cm) chromite schlieren, some 0·5–1 m long, in dunite (sample 6VA). Rare examples of massive ore-forming veins up to 5 cm thick and 50 cm long have been found (sample NT10). Another feature typical of the Nizhny Tagil chromitite is a brecciated texture, consisting of small nodules and angular blocks of dunite cemented by massive chromite.

The studied pyroxenite (sample NT12) has an adcumulate texture, comprising 90 vol. % clinopyroxene and rare olivine, with minor magnetite. The chromitite sample (KM10) is from a thin (5 cm) chromite schlieren in dunite. A similar sample was used for *in situ* analysis of Os. This type of chromite is common in the Pt-rich zones that have been exploited for primary platinum ore.

Mineral chemistry and conditions of formation

Forsterite (Fo) contents in olivine range from 0·89 to 0·92 in dunite (Ivanov, 1997; Augé *et al.*, 2005). For olivine from the chromium-rich samples (1 wt % < Cr_2O_3 < 26 wt %) the Fo contents are higher, ranging from 0·90 to 0·94 (Ivanov, 1997; Augé *et al.*, 2005). The average CaO content of the olivine is 0·2 wt % and NiO = 0·18–0·20 wt % (Ivanov, 1997). Chrome spinel coexisting with olivine has variable Cr_2O_3 contents ranging from 24 to 55 wt %, less than 10 wt % Al_2O_3 and 1 wt % TiO_2 (e.g. Ivanov, 1997; Augé *et al.*, 2005; Shmelev, 2007). The Cr/(Cr + Al) atomic ratio varies from 0·70 to 0·84, with an average of 0·80.

Clinopyroxene in the Nizhny Tagil Complex occurs as a rare intercumulus phase in the dunite and as a cumulus phase in the wehrlite and pyroxenite rim. It is an Mg-rich diopside showing slight Fe enrichment from the dunite to the wehrlite and pyroxenite (Augé *et al.*, 2005), with the Fo contents ranging from 0·48 to 0·52. The SiO_2 proportion decreases and Al_2O_3 proportion increases in clinopyroxene from the different lithologies from the dunite towards the wehrlite and pyroxenite (Fig. 3).

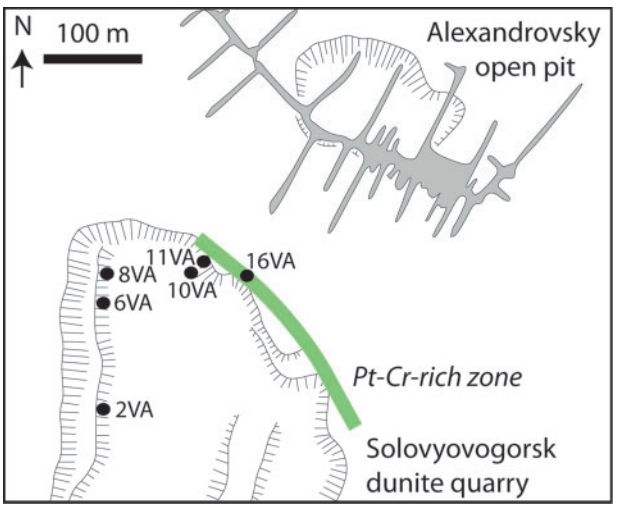

Fig. 2. Sample locations within the Solovyovogorsk quarry (number 5 in Fig. 1). Projection of the underground workings is shown for Alexandrovsky.

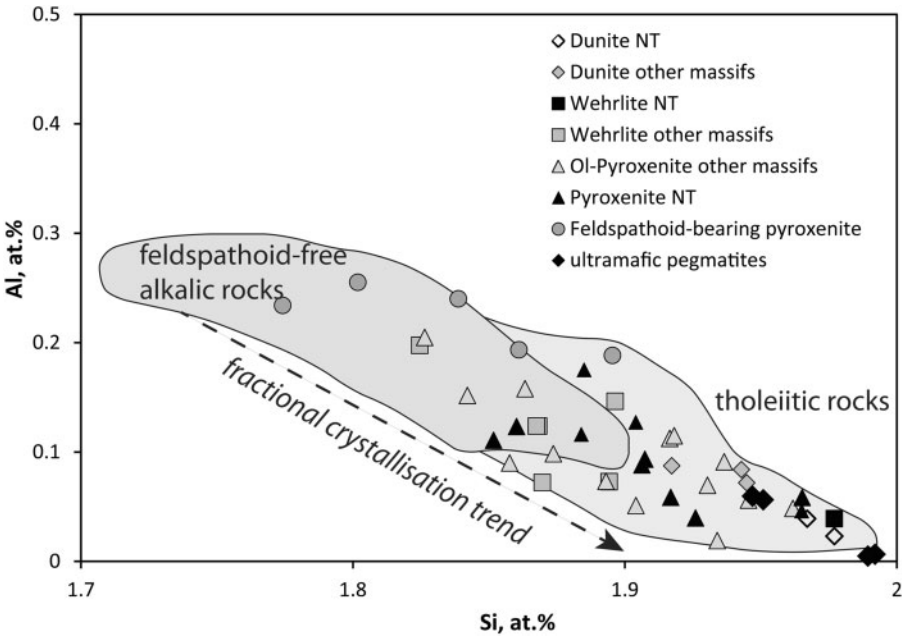

Fig. 3. Relation between the atomic proportions of Si and Al in clinopyroxenes from the different lithologies in the Nizhny Tagil and other zoned clinopyroxenite–dunite massifs in the Urals; data from Ivanov (1997) and Augé *et al.* (2005). The fields of clinopyroxenes from tholeiitic rocks and feldspathoid-free alkalic rocks are from Kushiro (1960). A schematic fractional crystallization trend is indicated. NT, Nizhny Tagil.

The Cr-spinel from the Nizhny Tagil massif has a high Cr number [Cr/(Cr + Al) = 0·70–0·84], high Ti and high Fe^{3+} substituting for Cr at a relatively low Al content, suggesting crystallization under high-fO_2 conditions (Garuti, 2014). The redox state of Cr-spinel in equilibrium with olivine within the dunites was estimated at +2·7, relative to fayalite–magnetite–quartz (FMQ), by Chashchukhin *et al.* (2014) based on Mössbauer spectroscopy of Cr-spinel. Significantly, the oxygen fugacity in chromitites with low PGE contents is virtually identical to that of the host dunites, whereas it is significantly higher (by 1·5–2 orders of magnitude) in chromitites with high PGE contents.

Olivine crystallization temperatures have been estimated in a range from 1430 to 1360°C, with a final crystallization temperature of 1280°C (Simonov *et al.*, 2013) based on melt inclusion compositions. Accessory Cr-spinel crystallized over a range of temperatures from 1345 to 1310°C. The lower temperatures were obtained for olivine–Cr-spinel equilibrium ($T^{Ol–Sp}$) by Chashchukhin *et al.* (2014) based on the oxidation state of Cr-spinel measured using Mössbauer spectroscopy. The dunites show significant variations in $T^{Ol–Sp}$, decreasing from fine-grained marginal lithologies (1050–1150°C) to the coarse-grained dunite core (~1000°C). The lowest $T^{Ol–Sp}$ was recorded within high-PGE chromitites (~900°C).

ANALYTICAL METHODS

Major and trace elements

Whole-rock major and trace element concentrations were determined at the Service d'Analyse des Roches et des Minéraux (SARM) at the Centre de Récherche Pétrographiques et Géochimique (SRPG-CNRS, Nancy, France). Analyses of standards and international reference materials [Basalt BR; peridotite UB-N ($n = 2$); diorite DRN] were within the standard deviation of values reported at http://helium.crpg.cnrs-nancy.fr/SARM/pages/geostandards.html. Major element analysis was performed by inductively coupled plasma optical emission spectrometry (ICP-OES) after alkaline fusion with lithium borate and nitric acid dissolution. The analytical uncertainty for this technique is <5% for elements with concentrations exceeding 0·5 wt %, and <15% for element concentrations below 0·5 wt %. Trace elements were measured by inductively coupled plasma mass spectrometry (ICP-MS). The same reference materials were run during the trace element analysis, with results within the accepted standard deviation values reported on the SARM website. At a concentration level above 50 ppm (i.e. for most common concentrations of Co, Ni and Cr), the precision and accuracy are <5%. V and Sc have concentrations between 1 and 100 ppm in the samples studied, with an analytical uncertainty of <15%. The rare earth elements (REE) and other trace element concentrations are generally lower than the detection limit, as indicated in Table 1.

Platinum-group elements

The PGE and Cr in whole-rock samples were analyzed by ICP-MS at the Commissariat à l'Energie Atomique (CEA) laboratory (Saclay, France). Approximately 10 g of sample powder was fused with sodium peroxide in a zirconium crucible and dissolved with a solution

Table 1: Whole-rock major and trace element data for Nizhny Tagil and Kachkanar (KS28) dunite and pyroxenite samples

Sample:	2VA	8VA	10VA	11VA	9VA	16VA	KS28	NT12
Massif:	NT	NT	NT	NT	NT	NT	Kachkanar	NT
Lithology:	Dunite	Dunite	Dunite	Dunite	Dunite	Dunite	Dunite	Pyroxenite
SiO_2	35·43	33·66	34·82	33·30	35·60	32·82	38·61	46·01
TiO_2	<0·02	<0·02	<0·02	<0·02	<0·02	<0·02	<0·02	0·35
Al_2O_3	0·04	0·06	0·04	0·07	0·04	0·09	0·13	2·51
Fe_2O_3	7·67	7·36	8·00	7·51	7·89	7·20	8·54	12·28
MnO	0·15	0·15	0·16	0·15	0·16	0·14	0·17	0·21
MgO	44·23	42·11	43·19	41·75	44·33	41·17	43·59	20·21
CaO	0·29	0·22	0·25	0·20	0·24	0·20	0·27	17·29
Na_2O	<0·01	<0·01	<0·01	<0·01	<0·01	<0·01	<0·01	0·22
P_2O_5	0·09	0·04	0·08	0·07	0·05	<0·04	<0·04	<0·04
LOI	11·73	15·73	12·98	17·10	12·17	18·43	7·96	0·51
ppm								
Sc	3·48	3·19	3·3	3·79	3·99	3·05	3·94	84·28
V	1·968	2·736	2·31	2·984	2·135	3·082	6·089	139·8
Cr	1688	2629	2132	3125	1972	3381	3338	964·2
Co	108·9	103·3	106·9	101·9	102·2	100·1	122·8	71·12
Ni	1050	982·2	1032	857·6	1051	995·8	1129	212·7
Cu	5·607	<5	<5	<5	<5	<5	10·77	9·219
Zn	44·1	44·26	46·78	42·1	42·82	41·01	56·63	51·12
Ga	0·491	0·546	0·489	0·542	0·477	0·531	0·745	5·526
Ge	0·95	0·874	0·929	0·882	0·883	0·894	1·14	2·047
Rb	*<0·4*	*<0·4*	*<0·4*	*<0·4*	*<0·4*	*<0·4*	*<0·4*	*<0·4*
Sr	*<2*	*<2*	*<2*	*<2*	*<2*	*<2*	6·989	159·9
Y	*<0·2*	*<0·2*	*<0·2*	*<0·2*	*<0·2*	*<0·2*	*<0·2*	4·391
Zr	*<1*	*<1*	*<1*	*<1*	*<1*	*<1*	*<1*	6·548
Ba	*<1·6*	*<1·6*	*<1·6*	*<1·6*	2·825	1·617	3·909	2·504
La	0·13	*<0·09*	*<0·09*	*<0·09*	*<0·09*	*<0·09*	0·114	1·266
Ce	0·233	*<0·14*	*<0·14*	*<0·14*	*<0·14*	*<0·14*	0·15	3·98
Pr	0·025	*<0·015*	*<0·015*	*<0·015*	*<0·015*	*<0·015*	0·029	0·702
Nd	0·076	*<0·06*	*<0·06*	*<0·06*	*<0·06*	*<0·06*	0·102	3·814
Sm	*<0·015*	*<0·015*	*<0·015*	*<0·015*	*<0·015*	*<0·015*	0·018	1·196
Eu	*<0·005*	*<0·005*	*<0·005*	*<0·005*	*<0·005*	*<0·005*	0·007	0·411
Tb	*<0·003*	*<0·003*	*<0·003*	*<0·003*	*<0·003*	*<0·003*	*<0·003*	0·171
Gd	*<0·013*	*<0·013*	*<0·013*	*<0·013*	*<0·013*	*<0·013*	0·014	1·176
Dy	*<0·01*	*<0·01*	*<0·01*	*<0·01*	*<0·01*	*<0·01*	0·014	0·945
Ho	0·002	*<0·002*	*<0·002*	*<0·002*	0·002	*<0·002*	0·004	0·183
Er	*<0·01*	*<0·01*	*<0·01*	*<0·01*	*<0·01*	*<0·01*	0·012	0·429
Yb	0·011	0·01	0·01	0·008	0·01	0·008	0·015	0·361
Lu	*<0·003*	*<0·003*	*<0·003*	*<0·003*	*<0·003*	*<0·003*	0·003	0·053
Hf	*<0·03*	*<0·03*	*<0·03*	*<0·03*	*<0·03*	*<0·03*	*<0·03*	0·331
Ta	*<0·01*	*<0·01*	0·016	0·044	*<0·01*	*<0·01*	*<0·01*	*<0·01*
Pb	<0·7	<0·7	<0·7	<0·7	<0·7	<0·7	<0·7	0·9125

wt % - Weight Percent; ppm - Parts Per Million; LOI - Loss On Ignition.

acidified with HCl. Precipitation was achieved by reduction of the PGE with Sn^{2+}, using selenium and tellurium as carriers in the presence of a catalyst, according to the method of Amossé (1998). The extraction yields obtained by this method are between 95 and 100% for PGE. Measurements of PGE concentrations in the extraction residues were made using ICP-MS. The blanks for this procedure (in ppb) are 0·02 for Ir, 0·03 for Ru and Rh, 0·25 for Pt and 0·15 for Pd. The instrumental limits of detection (in ppb) are 0·006 for Ir, 0·003 for Ru and Rh, 0·008 for Pt and 0·02 for Pd. Os was analysed in the same samples at the same time as Os isotopes using an isotope dilution thermal ionization mass spectrometry (ID-TIMS) technique. Blank contributions for the PGE varied between 0·3 and 85%.

Platinum-group minerals

Initially, the chemical compositions of PGM grains were analysed quantitatively with an ARL-SEMQ microprobe with four wavelength-dispersive spectrometers (WDS) at the Institute of Geological Sciences, University of Leoben (Austria). Quantitative WDS analyses were performed at 25 kV accelerating voltage and 20 nA sample current, with a beam diameter of about 1 μm. The following X-ray lines and standards were used: OsMα, IrLα, RuLα, RhLα, PtLα, PdLβ, NiKα (all native elements standards), FeKα, CuKα, SKα (all chalcopyrite). Corrections were performed for the interferences involving Ru–Rh, Ru–Pd and Ir–Cu. Approximately 150 analyses were obtained on selected PGM grains. In addition, PGM with analysis spots produced during laser ablation multicollector inductively coupled plasma mass spectrometry (LA-MC-ICP-MS) analysis were investigated using a JEOL-JSM6390LV scanning electron microscope and a CAMECA SX-100 electron microprobe at the Institute of Geology and Geochemistry, Ural Branch of Russian Academy of Sciences (RAS) in Ekaterinburg (Russia).

Re–Os isotopes

Whole-rocks

Re and Os concentrations and Os isotopic composition were analysed in two laboratories using different analytical protocols. The first batch of seven samples was analysed at IPGP (Institut de Physique du Globe, Paris VI University). The samples were prepared for Re–Os analysis using a low-temperature acid digestion technique. This method was developed by Birck *et al.* (1997) to achieve extremely low procedural blanks at a few tens of parts per trillion (ppt, 10−12 g g^{-1}), levels necessary for processing silicate-bearing rock samples with low metal abundance. Approximately 0·2 g of dunite and 0·5 g of pyroxenite rock sample powders were spiked with a mixed ^{190}Os–^{185}Re spike and then dissolved with HBr and HF in a Teflon bomb at 145°C. After evaporation, Os was oxidized to OsO_4 in a nitric acid solution containing chromium trioxide to ensure spike–sample equilibration. Finally, Os was extracted in liquid bromine and purified by a microdistillation technique. The supernate was reduced by ethanol and Re was extracted and purified by liquid–liquid extraction with iso-amylic alcohol and 2N HNO_3. The purified Os and Re fractions were loaded on Pt and Ni filaments, respectively, and measured using negative thermal ionization mass spectrometry (N-TIMS) on a Finnigan MAT-262, as described by Birck *et al.* (1997). The IPGP Merck Os standard yielded $^{187}Os/^{188}Os = 0{\cdot}1746 \pm 8$ ($n = 4$, 2σ SD) during the period of the measurements and the total procedural blank for Os was 0·47–0·53 pg ($n = 2$). The $^{187}Os/^{188}Os$ ratios for the blanks ranged between 0·129 and 0·142. The Re blanks ranged between 8 and 10 pg. Because the total blanks for both Re and Os were run as part of each batch of dissolutions, the appropriate blank correction was applied for each batch of samples.

The second batch of samples (chromitite KM10, chromite-bearing dunite NT10, and dunite 6VA) were analysed at the John de Laeter Centre for Isotopic Research at Curtin University in Perth. To achieve a complete digestion of refractory chromium spinel and associated platinum-group alloys, we used the Carius tube digestion method (Shirey & Walker, 1995). For dunites 1·7–2·8 g of whole-rock sample powder and 0·33 g of pure chromite separate were mixed with appropriate amounts of ^{185}Re and ^{190}Os spikes. The acid digestion was carried out using concentrated acids (3 ml of purged double-distilled HNO_3 and 6 ml of triple-distilled HCl). This mixture was chilled and sealed in previously cleaned Pyrex™ borosilicate Carius tubes (CT) and heated to 220°C for 60 h. Osmium was extracted from the acid solution by chloroform solvent extraction (Cohen & Waters, 1996), then back-extracted into HBr, followed by purification via microdistillation (Birck *et al.*, 1997). The supernate was reduced by ethanol and Re was extracted and purified by liquid–liquid extraction with iso-amylic alcohol and 2N HNO_3. The analysis of UB-N peridotite reference material gave $^{187}Os/^{188}Os$ of $0{\cdot}1272 \pm 0{\cdot}0005$ (reference value is $0{\cdot}1278 \pm 0{\cdot}0002$; Meisel *et al.*, 2003) with an Os concentration of 3·36 ppb (average for Carius tube method is 3·23 ppb; Meisel *et al.*, 2003).

The purified Os and Re fractions were loaded onto Pt filaments, and measured using N-TIMS on a ThermoFisher Triton® mass spectrometer using a secondary electron multiplier detector at the John de Laeter Centre, Curtin University. The measured isotopic ratios were corrected for mass fractionation using $^{192}Os/^{188}Os = 3{\cdot}092016$, as well as spike and blank contributions. The internal precision of measured $^{187}Os/^{188}Os$ in all samples was better than 0·15% (2σ SD). To monitor long-term instrument reproducibility an AB-2 Os standard (University of Alberta) was analysed. The AB-2 Os standard yielded $0{\cdot}10687 \pm 0{\cdot}00012$ ($n = 2$, 2σ SD) during the period of the measurements, which is consistent with data reported by Selby & Creaser (2003) ($0{\cdot}106838 \pm 0{\cdot}00004$, $n = 2$). An in-house Re standard solution gave $^{185}Re/^{187}Re = 0{\cdot}59870 \pm 0{\cdot}0008$ ($n = 2$, 2σ SD). The total procedural blank for Os was 0·50 pg ($n = 2$) and 5·8 pg for Re. The $^{187}Os/^{188}Os$ ratios for the blank were $0{\cdot}219 \pm 0{\cdot}043$ ($n = 2$). For the whole-rock samples, the total Os analytical blank on average constitutes less than 1·2% (0·04% in average) of the total Os analysed.

In situ *Re–Os analysis*

LA-ICP-MS analysis of selected PGM grains was performed in the Geochemical Analysis Unit at GEMOC–CCFS, Macquarie University, Sydney. The details of the method and operating parameters for *in situ* Re–Os isotope analysis of high-Os minerals (i.e. PGM) have been described previously (e.g. Pearson *et al.*, 2002; González-Jiménez *et al.*, 2012), and are briefly outlined below.

The technique uses a New Wave/Merchantek UP 213 laser microprobe with a large-format cell attached to a Nu Plasma MC-ICP-MS system. During the analysis of PGM all ion beams were collected in Faraday cups. The laser was fired at a frequency of 4 Hz, with energies of 1–2 mJ per pulse and a spot size of 15 μm. A standard NiS bead (PGE-A) with 199 ppm Os (Lorand & Alard, 2001) and $^{187}Os/^{188}Os = 0{\cdot}1064$ (Pearson *et al.*, 2002) was analyzed between samples to monitor any drift in the Faraday cups. The overlap of ^{187}Re on ^{187}Os was corrected by measuring the ^{185}Re peak and using $^{187}Re/^{185}Re = 1{\cdot}6742$. Data were collected using the Nu Plasma time-resolved software, which allows the selection of the most stable intervals of the signal for integration. The external reproducibility of $^{187}Os/^{188}Os$ for the PGE-A standard during the period of measurements was 0·00013 (2σ SD; $n = 15$) with a mean value of 0·10652.

Rhenium depletion ages (T_{RD}) were calculated assuming that the $^{187}Re/^{188}Os$ ratio of the peridotites was equal to zero at the time of melting. This approach allows later modification of the Re/Os ratio related to tectonic emplacement and alteration processes to be ignored. The T_{RD} (Table 2) were calculated relative to

Table 2: Re–Os and PGE concentrations and isotope data for dunites and pyroxenite from the Nizhny Tagil massif

Sample	Lithology	Cr_2O_3 (wt %)	Ir (ppb)	Ru (ppb)	Rh (ppb)	Pt (ppb)	Pd (ppb)	Re (ppb)	Os (ppb)	$^{187}Os/^{188}Os$	$^{187}Re/^{188}Os$	T_{RD}^a (Ma)	T_{RD}^b (Ma)
UB-N	Per							0·251	3·36	0·1272 ± 5	0·36		
2VA	D	0·31	0·5	<1·9	0·85	0·3	<2·2	0·609	0·043	0·1332 ± 17	0·133		
6VA^{CT}	D + Cr	8·68	9·4	46	6·5	2·1	<2·2	0·702	3·932	0·1237 ± 10	7·16	696	624
8VA	D	0·45	0·7	<1·9	1·2	0·4	<2·2	0·887	0·660	0·1160 ± 16	0·116	1766	1701
9VA	D	0·34	0·6	<1·9	0·99	0·4	<2·2	1·304	0·069	0·1266 ± 15	91·15	287	213
10VA	D	0·34	0·4	<1·9	0·97	1·0	<2·2	0·647	0·074	0·1250 ± 14	42·48	513	440
11VA	D	0·48	0·7	2·3	2·4	98	<2·2	0·241	3·427	0·1239 ± 4	0·34	667	596
16VA	D	0·53	1·0	<1·9	1·5	14	<2·2	0·211	0·580	0·1233 ± 6	2·68	752	680
16VA*	D							1·377	2·485	0·1230 ± 2	1·77	794	723
NT10^{CT}	D + Cr							0·197	0·604	0·1239 ± 10	1·58	667	596
NT12	Px	0·16	0·2	<1·9	0·83	11	<2·2	0·211	0·639	0·1250 ± 16	50·22	513	440
KM10^{CT}	Cr		60	29	80	1297	11·7		1·323	0·1215 ± 6	2·97	1,003	934

Per, peridotite; D, dunite; Cr, chromitite; Px, pyroxenite. The T_{RD} were calculated for two distinct reservoirs: (1) CHUR reservoir (T_{RD}^a) with $^{187}Re/^{188}Os = 0·423$ (Chen *et al.*, 1998), initial $^{187}Os/^{188}Os$ of 0·09531, resulting in present-day $^{187}Os/^{188}Os = 0·12863$; (2) Enstatite Chondrite Reservoir (ECR) using $^{187}Re/^{188}Os = 0·421$ (Walker *et al.*, 2002) and present-day $^{187}Os/^{188}Os = 0·1281$ (T_{RD}^b). It should be noted that the estimation of T_{RD} using a Depleted Mantle reservoir cannot be done accurately because of the great variations in $^{187}Re/^{188}Os$ ratio (0·06–1; e.g. Pearson *et al.*, 1995). The PGE data are from Augé *et al.* (2005).
* - duplicate; CT - digestion was done by Carius Tube method.

two distinct reservoirs: (1) a CHUR reservoir (T_{RD}^a) with $^{187}Re/^{188}Os = 0·423$ (Chen *et al.*, 1998) and initial $^{187}Os/^{188}Os$ of 0·0953 ± 0·0013, resulting in present-day $^{187}Os/^{188}Os = 0·12863 \pm 0·00046$; (2) an Enstatite Chondrite Reservoir (ECR) using $^{187}Re/^{188}Os = 0·421 \pm 0·013$ (Walker *et al.*, 2002) and present-day $^{187}Os/^{188}Os = 0·1281 \pm 0·0004$. The ^{187}Re decay constant of $\lambda = 1·666 \times 10^{-11}$ a^{-1} was taken from Smoliar *et al.* (1996).

RESULTS

Whole-rock compositions

The geochemical characteristics of the ultramafic rocks of the Nizhny Tagil massif differ significantly from those of ophiolite complexes and stratiform layered intrusions. Nonetheless, they have geochemical similarities to zoned Ural–Alaskan- and Aldan-type zoned complexes from other regions (e.g. Aldan Shield, Koryakiya, SE Alaska; e.g. Burg *et al.*, 2009).

Whole-rock analyses of the dunites (Table 1, Fig. 4) show that they are strongly depleted in elements such as Ca, Al, Ti and Na compared with estimates of fertile mantle composition (McDonough & Sun, 1995). Their Fe contents (average FeO = 7·8 wt %) are close to that estimated for Depleted MORB (mid-ocean ridge basalt) Mantle (DMM; the residue after extraction of MOR-type basalts; FeO = 8·1%, Salters & Stracke, 2004). In general, the composition of the dunites corresponds to an almost monomineralic Fo-rich olivine rock (Fig. 4b). Ultramafic rocks from the Uralian Kempirsai ophiolite massif have distinctly higher SiO_2 and lower MgO contents (Savelieva *et al.*, 1997; Fig. 4).

The clinopyroxenites are distinguished from the dunites by much higher Ca concentrations (CaO = 17·3 wt %, compared with 0·2–0·3 wt % in dunites), and a lower Mg/(Mg + Fe) atomic ratio (0·62 compared with 0·85 in dunites).

Trace elements

Trace element compositions of the dunites and the one pyroxenite sample studied are given in Table 1 and plotted in Fig. 5, with the elements arranged in sequence of their decreasing incompatibility during mantle partial melting processes and normalized to primitive mantle abundances (McDonough & Sun, 1995). The dunites are selectively enriched in highly incompatible elements including Ba, Rb, Th and U. The REE and other moderately incompatible elements are strongly depleted relative to primitive mantle values. The primitive mantle normalized REE patterns have a concave U-shape, with depletion in the middle REE (MREE) at 0·1 of chondrite-normalized values; such a shape is typical for peridotites from the Urals ophiolites (Melcher *et al.*, 1999), and for mantle xenoliths from subduction-zone settings (Grégoire *et al.*, 2001). The contents of compatible elements such as Cr and Co average 2488 and 104 ppm, respectively, close to those of depleted mantle (2500 and 106 ppm; Salters & Stracke, 2004).

The clinopyroxenite (Table 1, Fig. 5) shows a slight increase in chondrite-normalized REE abundances from La to Nd, gradually decreasing towards Lu. In general, the clinopyroxenite has a high normalized La/Yb ratio of 2–3.

PGE systematics

The Pt contents of the Nizhny Tagil dunite vary between 0·3 and 98 ppb (Table 2), and do not show any correlation with Cr content. Although the high-Pt sample was collected within the mineralized zone, other dunite samples in the vicinity of the mineralization have relatively low Pt contents. Excluding the single high value, the average Pt content for the dunite is 3·2 ppb ($n = 5$), with the majority of values below 1 ppb. The Pt contents of the chromitiferous dunite and chromite ores at Nizhny Tagil vary from 2·1 to 1297 ppb (Table 2). The pyroxenite has a slightly higher Pt content (11 ppb, Table 2) than the average dunite. The other PGE are also low in the dunite (Ir = 0·5–1·0 ppb, Ru < 1·9–2·3 ppb, Rh = 0·8–2·4 ppb, Pd < 2·2 ppb)

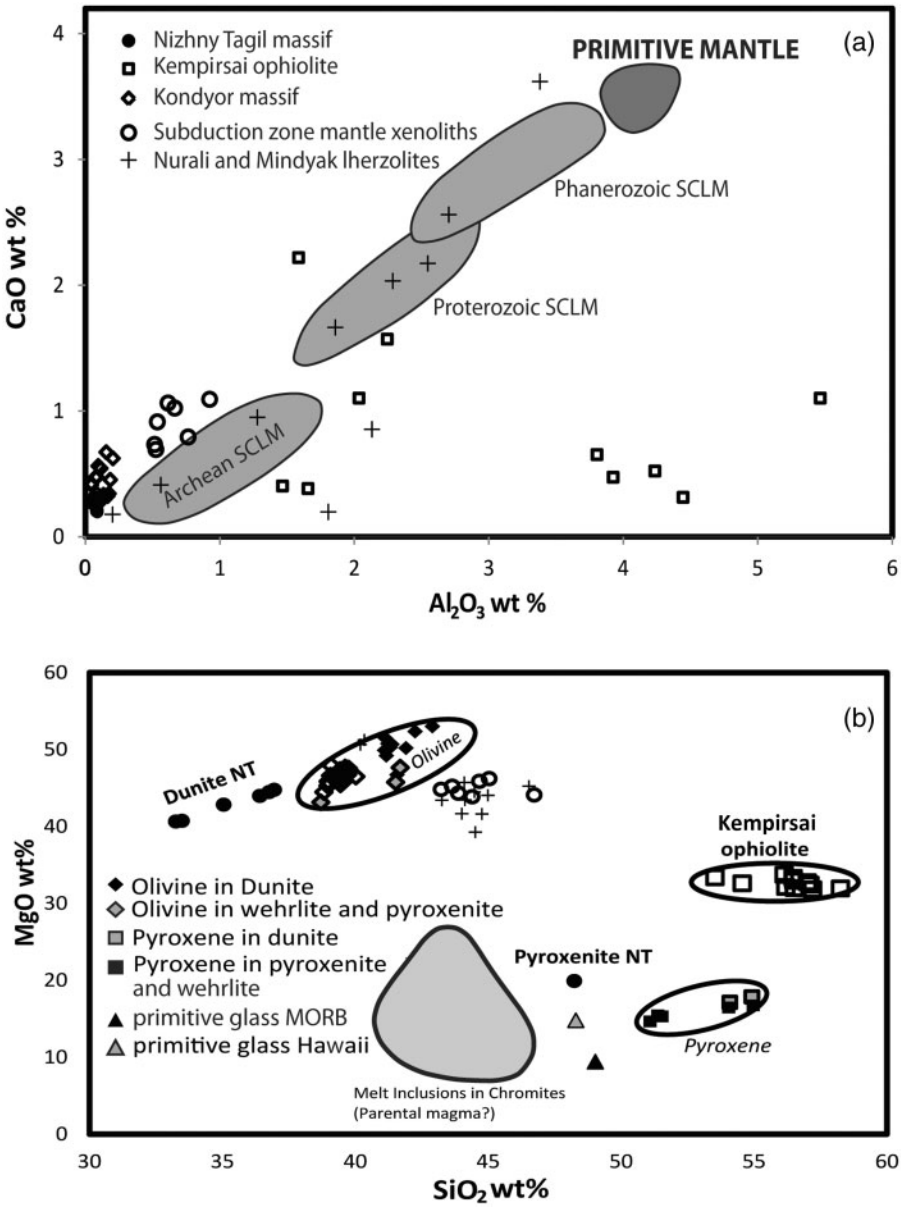

Fig. 4. (a) Al_2O_3 vs CaO for the rocks of the Nizhny Tagil massif (this study) compared with: (1) ultramafic portions of the Southern Urals lherzolite-bearing Nurali and Mindyak massifs (Tessalina *et al.*, 2007); (2) ultramafic rocks from the Southern Urals Kempirsai ophiolite (Savelieva *et al.*, 1997); (3) clinopyroxenite–dunite zoned Kondyor massif (Burg *et al.*, 2009); (4) ultramafic xenoliths from a subduction-zone setting in Papua New Guinea (McInnes *et al.*, 1999); (5) SCLM compositions for different geological periods (Griffin *et al.*, 2009). (b) SiO_2 vs MgO for the same rocks, with the addition of melt inclusion data from chromitites in Nizhny Tagil (light grey shaded field; Simonov *et al.*, 2013); primitive glass compositions from MORB and Hawaiian OIB (Simonov *et al.*, 2013, and references therein); microprobe data for olivine and pyroxene from different lithologies and pyroxenites from Nizhny Tagil are also plotted (Augé *et al.*, 2005).

and chromitiferous dunite (Ir = 9·4 ppb, Ru = 46 ppb, Rh = 2·1 ppb, Pd < 2·2 ppb; Table 2). The chromitite has higher contents of Ir, Ru and Rh (Table 2), but there is no significant correlation between the PGE. The overall primitive mantle normalized PGE abundance pattern for Nizhny Tagil ore-barren dunites shows a slight positive slope and is similar to that of dunites from the zoned massifs of the Aldan Shield (Malitch, 1990, 1998) and sub-arc mantle xenoliths (Fig. 6), and differs considerably from the 'flat' mantle-normalized PGE patterns of ophiolite-type peridotites.

The Pt/Pd ratios in chromitites from Nizhny Tagil range from 0·2 to 270·7 (Fig. 7), which are much higher than those of chromitites from Urals ophiolites (e.g. Kempirsai, Voikar-Syninsky, Rai-Iz) and about two orders of magnitude above chondritic values. The Pt/Pd ratios in ore-barren dunites with Cr_2O_3 contents below 0·5 wt % vary greatly, increasing toward the mineralized zone from subchondritic values of 0·3 to 13, with one value reaching 89 at 50 cm beneath the mineralized zone (Fig. 7). The pyroxenites exhibit high Pt/Pd ratios close to 10. These values are distinctly different from

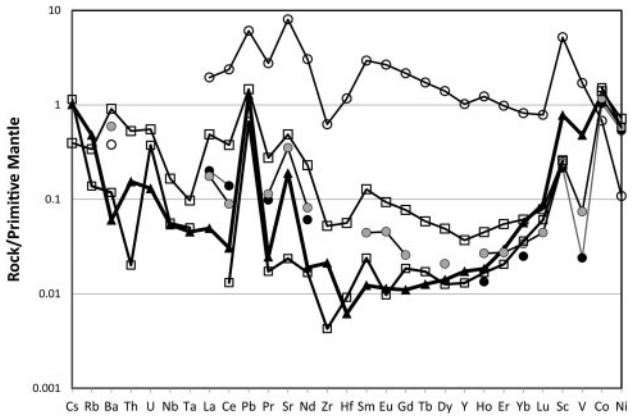

Fig. 5. Primitive mantle normalized trace element patterns for dunite from Nizhny Tagil (black filled circles) and Kachkanar (grey circles); pyroxenite (open circles) from the Nizhny Tagil massif is similar to that of Kondyor dunite (open squares; maximum and minimum values are shown Burg *et al.*, 2009) and mantle xenoliths from a subduction-zone setting in Papua New Guinea (filled triangles; Grégoire *et al.*, 2001). Normalizing values are after McDonough & Sun (1995).

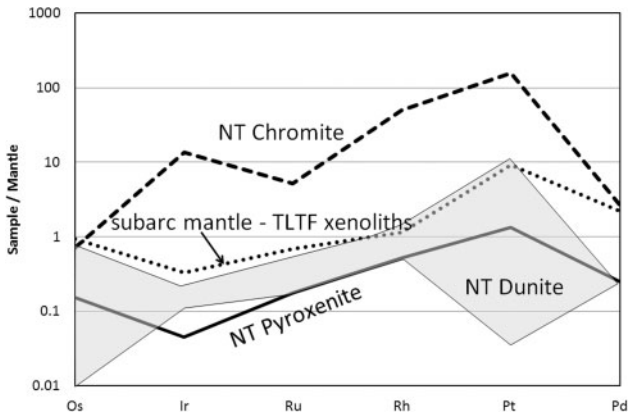

Fig. 6. Primitive mantle normalized PGE pattern for Nizhny Tagil (NT) ore-barren dunites (grey shaded field), pyroxenite and chromite compared with that for average harzburgitic mantle xenoliths from the Tabar–Lihir–Tanga–Feni (TLTF) arc in Papua New Guinea (McInnes *et al.*, 1999).

those in typical peridotites and ultramafic cumulates from Urals ophiolite complexes (e.g. Garuti *et al.*, 1997; Garuti, 2014), which have Pt/Pd ratios close to the primitive mantle value (1·9). Such enrichment in Pt is also a characteristic feature of sub-arc mantle, in which Pt/Pd ratios vary from 0·3 to 14·5 (with one value of 115), averaging 4·2 for Kamchatka mantle xenoliths (Kepezhinskas & Defant, 2001) and 9·9 for harzburgite xenoliths from Papua New Guinea (McInnes *et al.*, 1999). This range is similar to that observed for the Nizhny Tagil peridotites (Fig. 8).

Platinum-group minerals

The majority of PGM from the chromitites are dominated by Pt–Fe alloy grains (with sizes ranging from 10 to 2000 μm), with subordinate laurite, Os–Ir alloys and other PGM occurring as small inclusions in the Pt–Fe alloys

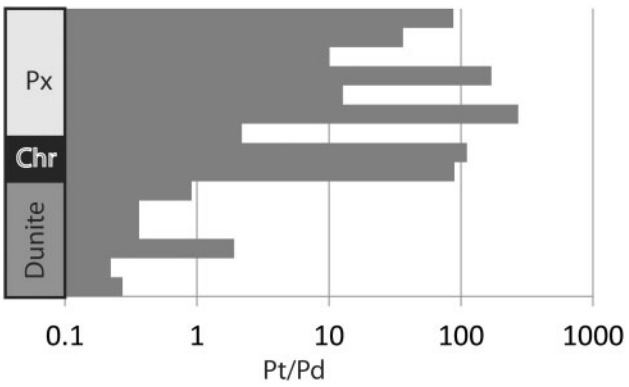

Fig. 7. Pt/Pd ratio variations across the Nizhny Tagil massif (from dunites to pyroxenites across the chromitites). Data from Augé *et al.* (2005).

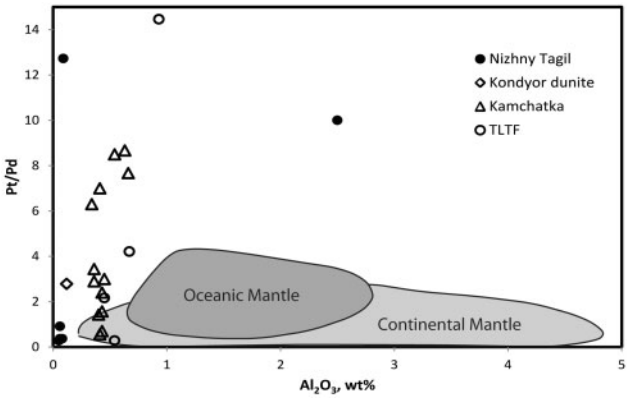

Fig. 8. Al_2O_3 concentrations (wt %) vs Pt/Pd ratio in Nizhny Tagil dunites and pyroxenite compared with that of continental mantle, oceanic mantle (Kepezhinskas & Defant, 2001, and references therein) and harzburgitic mantle xenoliths from the Tabar–Lihir–Tanga–Feni (TLTF) arc in Papua New Guinea (McInnes *et al.*, 1999) and Kamchatka mantle wedge harzburgites (Kepezhinskas & Defant, 2001) and dunite from Kondyor dunite-clinopyroxenite massif (Malitch, 1998).

(Fig. 9). Laurite, in addition to ruthenium and sulfur, contains minor amounts of osmium and iridium, varying in the range 0·38–1·24 at. % and 0–0·98 at. %, respectively (Table 3, analyses 3 and 6). According to the classification of Harris & Cabri (1991) Os–Ir–(Ru) alloys correspond to minerals of iridium and osmium (Fig. 10a, Table 3, analyses 7 and 8), and rarely to rutheniridosmine (Fig. 10a). Pt–Fe alloys show significant compositional variations. They are dominated by a Pt–Fe alloy with a composition close to Pt_2Fe [where Pt = PGE; Fe = (Fe + Cu + Ni)] relative to subordinate minerals of the tulameenite (Pt_2FeCu)–tetraferroplatinum (PtFe) series (Fig. 10b, Table 3, analyses 1, 2, 4 and 5).

Pressure estimation

The pressure of crystallization was estimated using the clinopyroxene compositions from Augé *et al.* (2005), following the method of Nimis & Ulmer (1998) and Nimis (1999); this yielded 18 ± 3 kbar for hydrous basaltic melts and 17 ± 2 kbar for melts of mildly alkaline

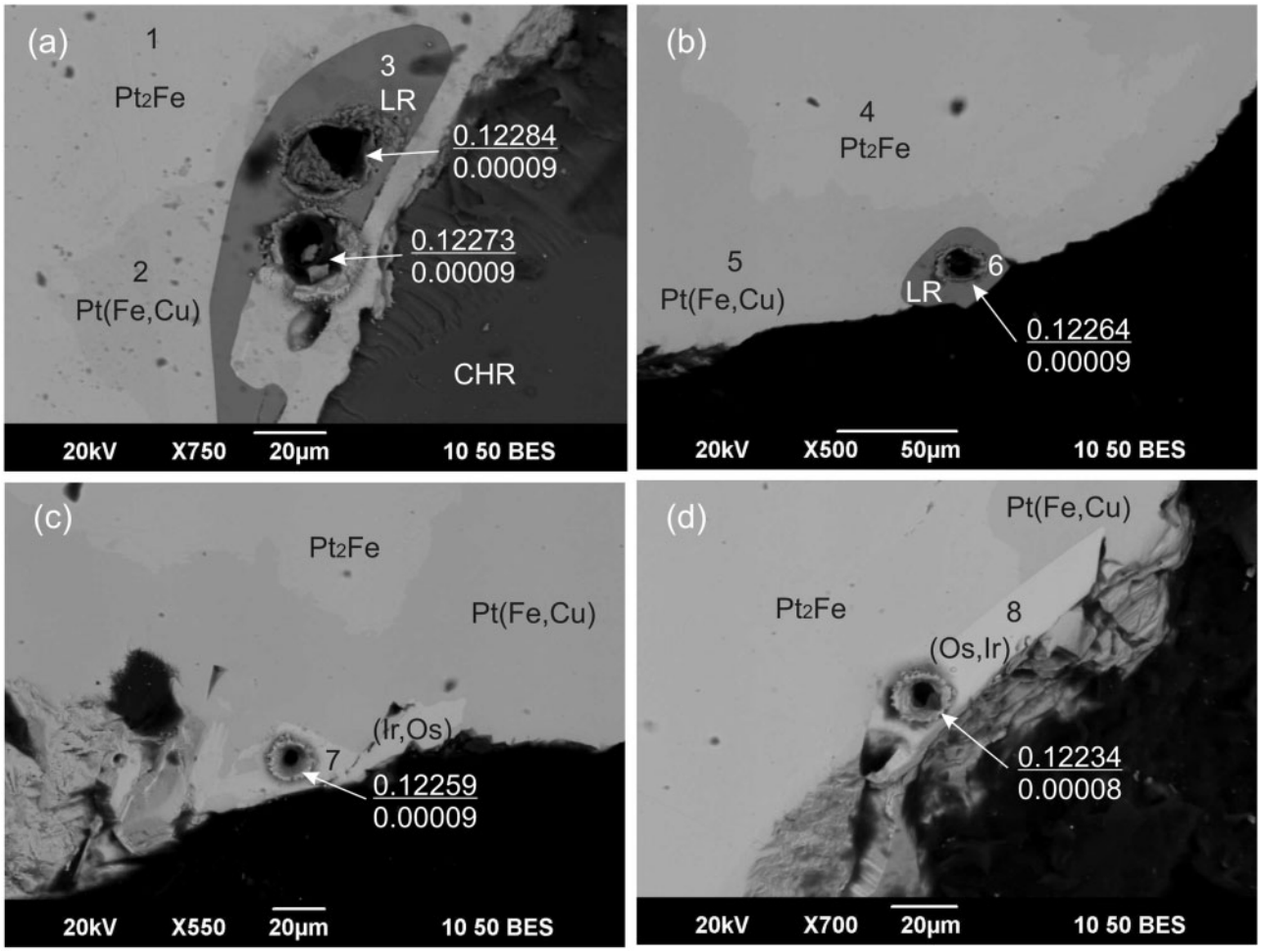

Fig. 9. Back-scattered electron images showing the textures of PGM in the chromitite of the Nizhny Tagil massif. Numbers 1–8 denote areas of electron microprobe analyses corresponding to the same numbers in Table 3. Pt_2Fe, ferroan platinum; Pt(Fe,Cu), solid solution series tetraferroplatinum (PtFe) - tulameenite (PtFe05Cu05); LR, laurite; (Ir,Os), osmian iridium; (Os,Ir), iridian osmium; CHR, chromite. Holes indicate the location of LA-MC-ICP-MS analyses; numbers in the numerator and denominator adjacent to the analysis pit correspond to the $^{187}Os/^{188}Os$ composition and the measurement error, respectively.

composition (Nimis, 1999). Clinopyroxenes from the dunites and pyroxenites give similar pressures.

Re–Os isotope systematics

Re–Os systematics of platinum-group minerals

Four laurite inclusions have $^{187}Os/^{188}Os$ values between 0·12256 ± 0·00006 and 0·12284 ± 0·00009 (Table 4), with a weighted mean of 0·12269 ± 0·00012 (2σ SD, $n = 4$), and $^{187}Re/^{188}Os$ lower than 0·00006, whereas Os–Ir alloys have $^{187}Os/^{188}Os$ values ranging from 0·12164 to 0·12259 with a mean of 0·12221 ± 0·00040 (1σ SD, $n = 4$). The Os isotope results indicate a restricted range of $^{187}Os/^{188}Os$ ratios for laurite and Os–Ir alloys (Table 4, Fig. 11) that are consistent, within uncertainty, with the 'unradiogenic' $^{187}Os/^{188}Os$ values previously reported for the chromitite (0·1215 ± 0·0006, Table 2; 0·1217, Malitch *et al.*, 2011). The average T_{RD} ages of laurite and Os–Ir alloys from the Nizhny Tagil massif vary between 816 and 984 Ma, averaging 871 ± 53 Ma (1σ SD; Table 4, Fig. 12) and correspond to a Neoproterozoic age (late Riphean according to the local stratigraphy).

Whole-rock Re–Os systematics

The Re and Os concentrations in the Nizhny Tagil dunites range from 0·21 to 1·4 ppb and from 0·04 to 3·9 ppb, respectively (Table 2). The Re concentrations are close to that of Depleted Mantle (0·157 ppb; Salters & Stracke, 2004), and about one order of magnitude higher than that of sub-arc depleted peridotites (0·04 ± 0·03, 1σ SD; McInnes *et al.*, 1999). On average, their Os contents are slightly lower than that of DMM (2·99 ppb; Salters & Stracke, 2004) and sub-arc mantle peridotites (3·85 ± 1·76, 1σ SD; McInnes *et al.*, 1999).

The $^{187}Os/^{188}Os$ ratios of whole-rock dunites from the Nizhny Tagil massif vary from 0·1160 to 0·1332, averaging 0·1247. Excluding the most radiogenic composition, the eight dunite samples display an average of 0·1232 ± 0·003 (1σ SD), which is slightly more

Table 3: Selected electron microprobe (WDS) analyses of PGM from the chromitite of the Nizhny Tagil massif

Analysis:	1	2	3	4	5	6	7	8
Sample:	223	223	223	254	254	254	247	244
Figure:	Fig. 9a	Fig. 9a	Fig. 9a	Fig. 9b	Fig. 9b	Fig. 9b	Fig. 9c	Fig. 9d
wt %								
Fe	11·85	13·68	0·00	12·01	14·59	0·00	0·00	0·00
Ni	0·33	0·42	0·00	0·63	0·39	0·00	0·00	0·00
Cu	0·78	9·12	0·00	0·92	8·26	0·00	0·00	0·00
Ru	0·00	0·00	54·92	0·00	0·00	59·68	6·43	7·08
Rh	0·46	0·74	0·00	0·75	0·80	0·00	0·00	0·00
Pd	0·00	0·00	0·00	0·00	0·00	0·00	0·00	0·00
Os	0·00	0·00	4·14	0·00	0·00	1·30	20·89	56·25
Ir	3·02	1·34	3·30	2·86	2·42	0·00	72·66	36·57
Pt	83·53	74·64	0·00	82·11	74·07	0·00	0·00	0·00
S	0·00	0·00	37·53	0·00	0·00	39·03	0·00	0·00
Total	99·97	99·94	99·89	99·28	100·53	100·01	99·98	99·90
at. %								
Fe	31·27	30·92	0·00	31·47	32·74	0·00	0·00	0·00
Ni	0·83	0·90	0·00	1·57	0·83	0·00	0·00	0·00
Cu	1·81	18·11	0·00	2·12	16·28	0·00	0·00	0·00
Ru	0·00	0·00	31·00	0·00.	0·00	32·54	11·54	12·60
Rh	0·66	0·91	0·00	1·07	0·97	0·00	0·00	0·00
Pd	0·00	0·00	0·00	0·00	0·00	0·00	0·00	0·00
Os	0·00	0·00	1·24	0·00	0·00	0·38	19·92	53·18
Ir	2·32	0·88	0·98	2·18	1·58	0·00	68·54	34·22
Pt	63·11	48·29	0·00	61·59	47·59	0·00	0·00	0·00
S	0·00	0·00	66·78	0·00	0·00	67·08	0·00	0·00
PGE total	66·09	50·07	33·22	64·84	50·14	32·92	100·00	100·00
Fe + Cu + Ni	33·91	49·93	0·00	35·16	49·86	0·00	0·00	0·00
Mineral formula	Pt_2Fe	Pt(Fe,Cu)	RuS_2	Pt_2Fe	Pt(Fe,Cu)	RuS_2	(Ir,Os)	(Os,Ir)

Pt_2Fe, ferroan platinum; Pt(Fe, Cu), minerals of the tulameenite–tetraferroplatinum series; RuS_2, laurite; (Os, Ir), Ir-bearing osmium; (Ir, Os), Os-bearing iridium.

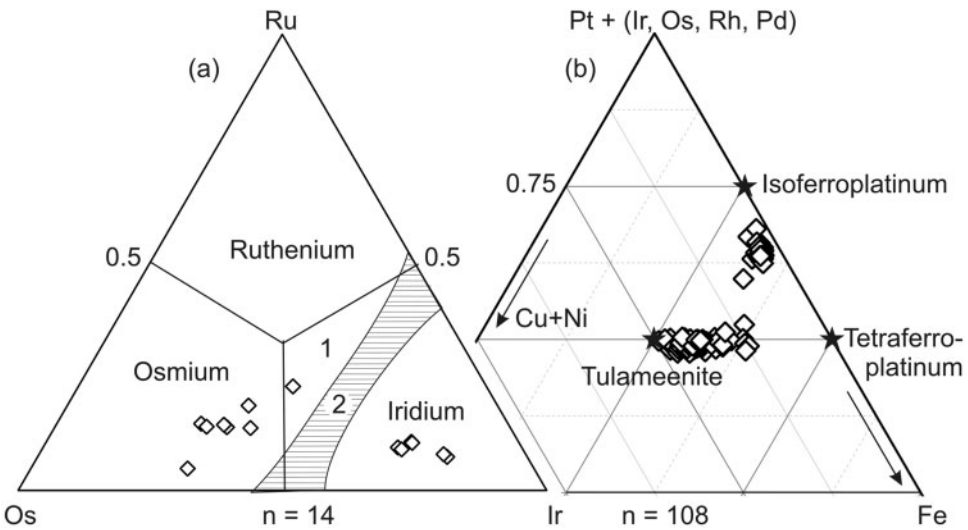

Fig. 10. Composition of Os–Ir and Pt–Fe alloys from the chromitite of the Nizhny Tagil massif (at. %): (a) Ru–Os–Ir plane; (b) [Pt + (Ir, Os, Rh, Pd)]–(Cu + Ni)–Fe plane. 1, rutheniridosmine; 2, miscibility gap.

radiogenic compared with the $^{187}Os/^{188}Os$ ratios of the PGM (0·1225 ± 0·0004, Table 4; 0·1217, Malitch *et al.*, 2011) and chromitites (0·1215 ± 0·0006, Table 2; 0·1245, Hattori & Hart, 1991), indicating that the Os budget in the dunites is largely controlled by PGM within chromite.

The variation of Re/Os ratios in the dunites and pyroxenite from the Nizhny Tagil massif is extremely large (from 0·07 to 18·8), exceeding the range for sub-arc mantle xenoliths (0·003–0·03; McInnes *et al.*, 1999). This difference is explained by much lower Re abundances in sub-arc mantle xenoliths, averaging 0·04 ppb for Papua New Guinea (McInnes *et al.*, 1999) and 0·05 ppb for Cascade arc xenoliths (Brandon *et al.*, 1996). A pronounced negative correlation exists between Re/Os and Pt/Pd (Fig. 13) for both datasets, with the Nizhny Tagil dunites having about two orders of magnitude higher Re/Os ratios.

Table 4: Osmium isotope composition and calculated model ages of laurite and Os–Ir alloys from the Nizhny Tagil massif

Sample no.	Mineral, rock	Atomic proportions	$^{187}Os/^{188}Os$	$T_{RD}{}^{a}$ (Ma)	$T_{RD}{}^{b}$ (Ma)
NT-223-1, Fig. 9a	Laurite	$(Ru_{0.93}Os_{0.03}Ir_{0.03})S_2$	0·12284(9)	816	745
NT-223-2, Fig. 9a	Laurite	$(Ru_{0.93}Os_{0.03}Ir_{0.03})S_2$	0·12273(9)	831	761
NT-254-1, Fig. 9b	Laurite	$(Ru_{0.99}Os_{0.01})S_2$	0·12264(9)	844	773
NT-240-1	Laurite	$(Ru_{0.99}Os_{0.01})S_2$	0·12256(6)	855	785
NT-226-1	Os-bearing iridium	$Ir_{73}Os_{16}Ru_{11}$	0·12225(10)	899	828
NT-228-1	Os-bearing iridium	$Ir_{46}Os_{30}Ru_{22}Fe_4$	0·12164(31)	984	914
NT-247-1, Fig. 9c	Os-bearing iridium	$Ir_{69}Os_{20}Ru_{11}$	0·12259(9)	851	780
NT-244-1, Fig. 9d	Ir-bearing osmium	$Os_{53}\ Ir_{34}Ru_{13}$	0·12234(8)	886	816
Average	PGM, $n = 8$		0·12245 ± 0·00038	871 ± 53	800 ± 53

Numbers in parentheses are 2σ error in the last decimal places of $^{187}Os/^{188}Os$ ratio; T_{RD}, model ages. $T_{RD}{}^{a}$ ages were calculated using the equation $T_{RD} = \left\{ \ln \left[\frac{\left(\frac{^{187}Os}{^{188}Os}\right)_{CHUR} - \left(\frac{^{187}Os}{^{188}Os}\right)_{Sample}}{\left(\frac{^{187}Re}{^{188}Os}\right)_{CHUR}} + 1 \right] \right\} / \lambda$, using CHUR values estimated by Chen *et al.* (1998) with $^{187}Re/^{188}Os = 0{\cdot}423$ and present-day $^{187}Os/^{188}Os = 0{\cdot}12863$. $T_{RD}{}^{b}$ model ages were calculated using ECR values estimated by Walker *et al.* (2002) using $^{187}Re/^{188}Os = 0{\cdot}421$ and present-day $^{187}Os/^{188}Os = 0{\cdot}1281$. ^{187}Re decay constant of $\lambda = 1{\cdot}666 \times 10^{-11}$ a^{-1} (Smoliar *et al.*, 1996) was used for calculations. Mean Os isotopic composition and T_{RD} ages were estimated as an average of all data points. Uncertainties on the means represent 1σ SD from the average values.

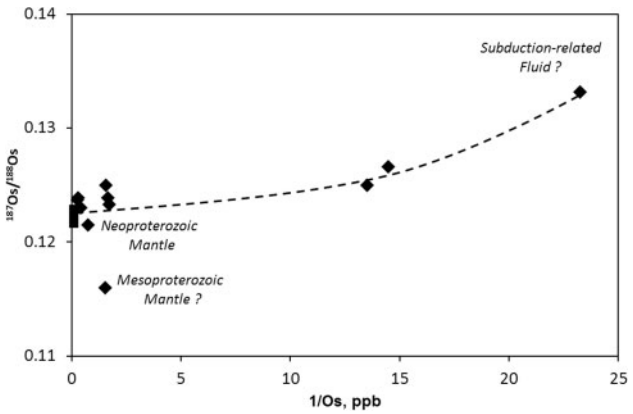

Fig. 11. $^{187}Os/^{188}Os$ vs 1/Os for dunites and pyroxenites from the Nizhny Tagil massif (filled diamonds). The trend of increasing Os isotopic composition with decreasing Os content (dotted line) can be ascribed to the admixture of subduction-related fluid. The least radiogenic $^{187}Os/^{188}Os$ value may indicate the ancient history of depletion. The *in situ* Os isotopic compositions of the PGM are also plotted (filled squares).

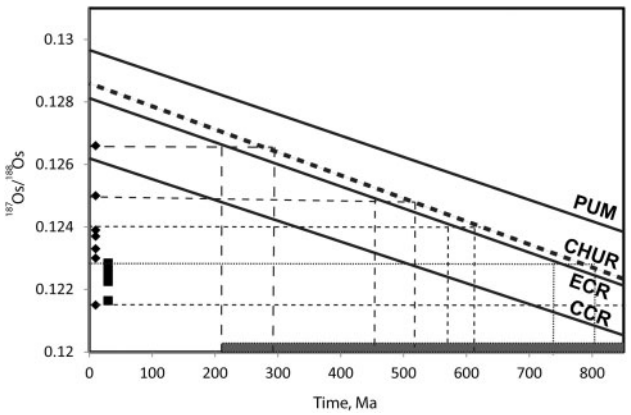

Fig. 12. Graphic representation of Os model ages for the Nizhny Tagil dunites and PGM estimated using different models for the Re–Os evolution of the convecting mantle [modified after Shi *et al.* (2007)]. Mantle evolution curves are defined as follows: CCR (Carbonaceous Chondrite reservoir) curve assumes that the Earth's mantle has an Os isotopic composition and Re/Os similar to that of carbonaceous chondrites ($^{187}Os/^{188}Os_{CC} = 0{\cdot}1262 \pm 0{\cdot}0006$, $^{187}Re/^{188}Os_{CC} = 0{\cdot}392 \pm 0{\cdot}015$; Walker *et al.*, 2002); ECR (Enstatite Chondritic Reservoir) curve is calculated using a present-day $^{187}Os/^{188}Os$ value of $0{\cdot}1281 \pm 0{\cdot}0004$ and $^{187}Re/^{188}Os = 0{\cdot}421 \pm 0{\cdot}013$ as measured in enstatite chondrites (Walker *et al.*, 2002); CHUR (Chondrite Uniform Reservoir) curve has initial $^{187}Os/^{188}Os$ of 0·09531, resulting in present-day $^{187}Os/^{188}Os = 0{\cdot}12863$ using $^{187}Re/^{188}Os = 0{\cdot}423$ (Chen *et al.*, 1998); PUM (Primitive Upper Mantle) curve has a present-day $^{187}Os/^{188}Os = 0{\cdot}1296 \pm 0{\cdot}0008$ and $^{187}Re/^{188}Os = 0{\cdot}42$. Grey band (X-axis) represent the time interval for Os model ages. Symbols as in Fig. 11.

DISCUSSION

Control on PGE distribution

The Pt budget is controlled by Pt–Fe alloys with compositions close to Pt_2Fe stoichiometry, which are well known from zoned clinopyroxenite–dunite massifs (Cabri *et al.*, 1996; Malitch & Badanina, 2015), ophiolite dunite–harzburgite complexes and layered ultramafic–mafic intrusions (Cabri *et al.*, 1996; Sluzhenikin, 2000). Os, Ir and Ru are present as Os–Ir–Ru mineral inclusions (alloys and sulphides) within Pt–Fe alloys, also a typical feature of zoned ultramafic massifs (Table 4; Cabri *et al.*, 1996; Malitch, 1999).

The positive Pt anomaly observed in the chromitites and dunites is considered to be a typical feature of Uralian–Alaskan-type complexes (e.g. Garuti *et al.* 1997). However, our dataset clearly shows variations in Pt concentrations increasing towards the mineralization zone by a factor of ~300 (from 0·3 to 98 ppb). The chondrite-normalized Pt abundances display both negative and positive anomalies, testifying to an effective mechanism for Pt fractionation during the formation of the UPB massifs. A factor of 100 difference in Pt concentrations in chromite-rich versus chromite-free rocks from Uralian–Alaskan-type massifs was reported by Crocket

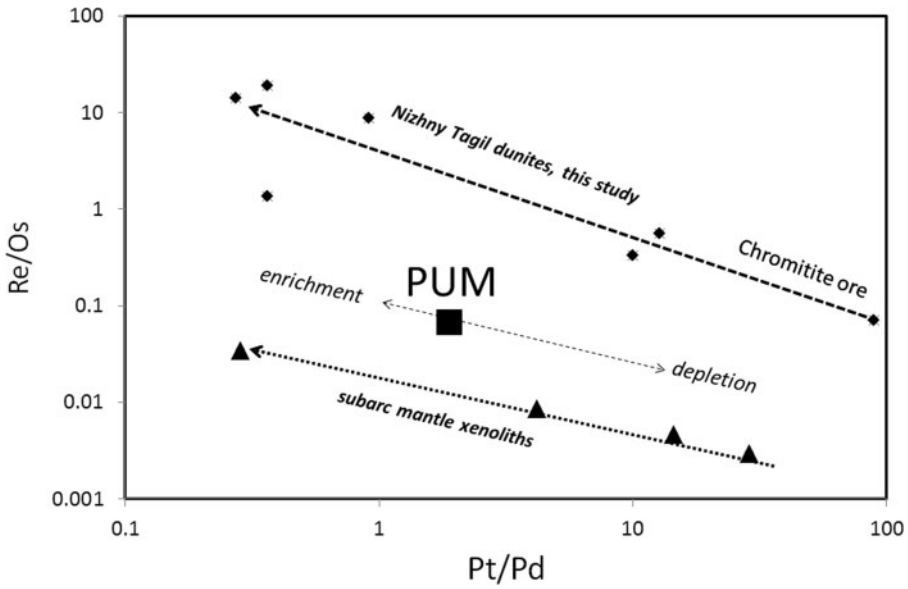

Fig. 13. Pt/Pd vs Re/Os for ultramafic rocks from the Nizhny Tagil massif (filled diamonds) and harzburgitic mantle xenoliths (filled triangles) from the Tabar–Lihir–Tanga–Feni arc in Papua New Guinea (McInnes *et al.*, 1999). The PUM (Primitive Upper Mantle) composition is indicated.

(1979). The average Pt content of the low-Cr dunites from Nizhny Tagil is 13 ppb (Augé *et al.*, 2005, $n = 17$), increasing to parts per million level (3·2 ppm) in chromiferrous dunite and chromitite (Augé *et al.*, 2005). The average value for low-Cr dunites is only twice as high as that of DMM (6·2 ppb; Salters & Stracke, 2004).

The Pt/Pd ratios show a pronounced negative correlation with Re/Os (Fig. 13), which can be attributed to compatible Pt and Os versus incompatible Re and Pd behavior. Compatible behavior of Pt is also consistent with the elevated MgO contents in dunites hosting Pt-bearing chromitites (Ivanov, 1997). Systematic Pt/Pd increases in the Nizhny Tagil rocks towards the chromite mineralized zone suggest that Pt–Pd fractionation may be related to the preferential retention of Pt in chromitites as Pt–Fe alloys (Augé *et al.*, 2005).

Control on Os isotopes

Ambiguity in the use and interpretation of whole-rock Os isotope data has arisen from a number of mineral-scale Os isotopic studies (e.g. Burton *et al.*, 1999; Alard *et al.*, 2002), which show the existence of inter-mineral Os isotope heterogeneity within single samples. These studies have demonstrated that the primordial Os isotopic signature of base-metal (BM) sulfides enclosed in silicates could easily be masked by highly radiogenic secondary BM sulfides, which cannot be evaluated from whole-rock Os isotopic ratios alone. This requires careful identification of the different minerals that govern the Os isotope systematics. This is a key tool in evaluating the significance of whole-rock Re–Os isotope signatures and model ages (Reisberg *et al.*, 2004).

The mobility of Os has been implicated for the radiogenic Os isotope signatures in mantle xenoliths from arc settings, including a number of modern island arcs (e.g. Widom *et al.*, 2003; Brandon *et al.*, 1996; McInnes *et al.*, 1999; Saha *et al.*, 2005). In general, the involvement of subduction-related fluids will increase the $^{187}Os/^{188}Os$ ratios of sub-arc mantle and its melting products (McInnes *et al.*, 1999; Saha *et al.*, 2005). For example, Kamchatka peridotite mantle xenoliths (Saha *et al.*, 2005) with higher Os contents (1·3–5·2 ppb) show a narrow $^{187}Os/^{188}Os$ range between 0·1182 and 0·1272, whereas xenoliths with lower Os contents (>1 ppb) show wider variation and more radiogenic $^{187}Os/^{188}Os$ values (0·1287–0·1585). These more radiogenic Os isotopic compositions in conjunction with He isotope data have been interpreted as a product of metasomatism by slab-derived fluids from subducting altered oceanic crust.

In our study, three dunite samples (2VA, 9VA, 10VA, Table 2) and one pyroxenite sample (NT12, Table 2) have chondritic (*c.* 0·124 at 400 Ma) and suprachondritic $^{187}Os/^{188}Os$ ratios up to 0·1332. These samples are characterized by relatively low Pt contents (0·3–1 ppb in dunites and 11 ppb in pyroxenite). The most radiogenic sample (2VA) is enriched in copper and LREE (above the detection limit, Table 1) compared with the other dunites. These features may indicate that, at least in part, its Os isotope composition can be ascribed to the involvement of more radiogenic subduction-related fluids, characteristic for sub-arc mantle (Fig. 11).

In contrast, the other five dunite samples and one chromite sample have subchondritic $^{187}Os/^{188}Os$ ratios of 0·1160–0·1239, overlapping the range of values for PGM (0·12164–0·12284, average 0·12245; Fig. 12). These values are similar to those of peridotites from the lherzolite-bearing massifs of Nurali and Mindyak in the Southern Urals (0·1191–0·1254; Tessalina *et al.*, 2007), as well as mantle peridotites from some modern island arcs such as Izu–Bonin–Mariana (0·1193–0·1274;

Parkinson *et al.*, 1998), characterized by involvement of an old mantle component.

The Re–Os model ages of the PGM (Table 4) average 871 ± 53 Ma (676 ± 56 Ma according to ECR), which resembles the Sm–Nd age of the Mindyak peridotites (882 ± 83 Ma) and Re–Os age of associated gabbros (804 ± 37 Ma) from the Southern Urals lherzolite-bearing massifs (Tessalina *et al.*, 2007), and records an unequivocally older melting event than that corresponding to Uralian island arc formation (*c.* 400 Ma). The T_{RD} model ages of dunite samples 6VA, 11VA and 16VA (667–794 Ma, or 596–723 Ma based on ECR, Table 2) possibly reflect the same event. The least radiogenic dunite (sample 8VA; Table 2) with $^{187}Os/^{188}Os$ of 0·1160 ± 16 gives the oldest T_{RD} model age of 1766 Ma (1701 Ma using ECR); this is even less radiogenic than the bulk of the Os isotopic compositions of the PGM (Table 2). However, because such a low value was encountered only in one sample, it is not considered to be statistically representative.

The inferred Re–Os model ages of PGM, dunites and chromitites are *c.* 300–400 Myr older than the melt depletion events that took place in the Tagil island arc (*c.* 400 Ma), which indicates that the mantle from which they were derived was already substantially more unradiogenic than DMM at the time of this melting event. This older mantle was involved in melting in a subduction zone at around 400 Ma, which is compatible with some of the Os isotopic data, and in agreement with the main age range (460–400 Ma) defined by different isotopic methods for the majority of the calc-alkaline volcanogenic complexes of the Tagil zone. The presence of ancient mantle in modern arcs has been previously demonstrated for the Izu–Bonin–Mariana arc (Parkinson *et al.*, 1998), where Proterozoic model ages have been established for fore-arc peridotites. These old ages were explained in terms of ancient melting events in the convecting upper mantle, which may result in less radiogenic Os isotope compositions than previously recognized (Parkinson *et al.*, 1998).

A simple model to explain subchondritic Os isotopic compositions requires an older melting event (*c.* 700–800 Ma) that strips out essentially all the Re and isolates the peridotites from the convecting upper mantle because they became less dense (highly depleted) relative to the fertile upper mantle. This density contrast will lead to stabilization of this mantle, making it difficult to subduct.

In conclusion, our new whole-rock and *in situ* Os isotope data support a model for a genetic difference between Uralian dunite cores and other mafic–ultramafic massifs (Malitch *et al.*, 2009, 2012; Krasnobaev & Anfilogov, 2014). We consider that the Uralian dunites incorporate ancient mantle domains that were tectonically integrated into the structure of the Uralian Platinum Belt.

Possible origin of UPB massifs

Despite a century of studies dedicated to understanding the zoned Ural–Alaskan-type complexes of the Urals, their nature and geodynamic setting remain controversial. Commonly accepted models describe the UPB as a chain of *in situ* intrusions in which dunite is assumed to represent a cumulate of mafic magma (e.g. Ivanov, 1997). This magmatic model of UPB massif formation has been further strengthened by the discovery of melt inclusions in chromian spinel (Simonov *et al.*, 2013). However, the lack of preserved magmatic structures or traces of primary layering and the absence of volcanic analogues has led many researchers to question the magmatic origin of the dunite–clinopyroxenite–gabbro complexes. For example, the increasing trend in Si proportions in clinopyroxenes from the Nizhny Tagil lithologies from the pyroxenites and wehrlites toward the dunites (Fig. 3) is opposite to that expected in a typical layered intrusion crystallized from the same batch of magma as fractionation proceeds, following the molecular concentrations of SiO_2 in the magma (Kushiro, 1960).

Approaching the genesis of the dunites as residues after melt extraction would not be possible without a comprehensive comparison with other types of peridotite, both from nature and experiments [see Herzberg (2004) for review]. This comparison is not easy, owing to the rarity of dunite lithologies among known peridotite types (Herzberg, 2004). Generally, peridotite residues display orthopyroxene enrichment to various degrees, which has been interpreted as reflecting an addition of basaltic melt to the residue. Indeed, most peridotites from subduction zones and ophiolites are too enriched in SiO_2 and too depleted in Al_2O_3 to be simple residues. The model residues for subduction-zone peridotites computed by Herzberg (2004) have ~5 wt % lower MgO contents compared with those of the Nizhny Tagil dunites.

Another way to reconstruct the origin of dunites as possible residues would be to identify the complementary liquids produced during the melting of the initial peridotite. The composition of such liquids may be best approximated by that of the pyroxenites that are always closely associated with dunites. The pyroxenite composition for Nizhny Tagil from our study (FeO 11 wt % and MgO 21 wt %; Table 1) fits well with the FeO and MgO contents of a melt in equilibrium with an olivine residuum at 1 GPa calculated for a peridotite with an Mg-number of 86·9 (Fig. 14; Herzberg & O'Hara, 2002; Herzberg, 2004). Such a liquid may be produced by equilibrium (Herzberg & O'Hara, 2002, fig. 5a) or accumulated fractional melting (Herzberg & O'Hara, 2002, fig. 6b) of depleted peridotite, generating in both cases pure olivine residues.

During accumulated fractional melting (AFM), successive melting events occur. Each time the liquid produced is completely removed from the residue, and the residue is melted again; each new melt is extracted and mixed with the previously formed melt (Herzberg & O'Hara, 2002). Such multi-stage events may be reflected in variable Fo contents in olivine (~17 Fo units across all lithologies in Nizhny Tagil), which has a short

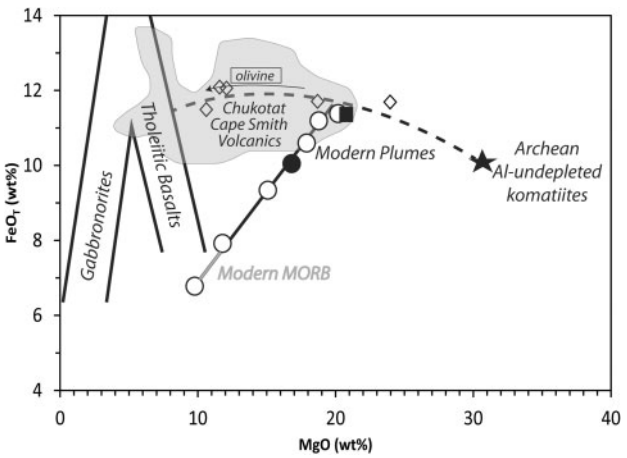

Fig. 14. MgO vs FeO_T for the Nizhny Tagil pyroxenite (filled square) and melt inclusions in chromian spinel (open diamonds; Simonov *et al.*, 2013) compared with Phanerozoic primary magmas [modified after fig. 14 of Herzberg (2004)]. Phanerozoic primary magmas are shown as open circles, with the exception of a model primary magma from the plume-related Ontong Java Plateau (filled circle; Herzberg, 2004). The field for Chukotat Group Cape Smith Volcanics is shown for comparison (Herzberg, 2004). The field labeled 'tholeiitic basalts' shows the trend of FeO_T enrichment for modern MORB as a result of fractionation of olivine + plagioclase ± augite. The field labeled 'gabbronorites' shows a trend of FeO_T depletion as a result of fractionation of plagioclase + augite + low-Ca pyroxene + magnetite in MORB. [For further explanation see Herzberg (2004).] Volcanic rocks from the early Proterozoic Cape Smith belt display olivine control that projects to inferred primary magmas with 18–20% MgO.

residence time in the magma (Danyushevsky *et al.*, 2002). This, in turn, will imply several magma injections, which incorporate previously formed olivine crystals. Repeated melting events (AFM) would also explain the increasing Pt/Pd ratios in ore-barren dunites towards the mineralized zone (Fig. 7).

The FeO_T and MgO contents of the derivative liquid should obey the linear relationship established for primary magmas: $FeO_T = 1{\cdot}933 + 0{\cdot}489MgO$ (Herzberg, 2004). In our case, MgO of 20·8 wt % (Table 1) corresponds to FeO_T of 11·4 wt % (Table 1), which is close to the calculated value of 12·1 wt %. Furthermore, the pyroxenite composition is characterized by a high MgO content (20–21 wt %) and lies close to the Phanerozoic primary magma composition established for modern plumes (Fig. 14; Herzberg & O'Hara, 2002; Herzberg, 2004). The compositions of melt inclusions in chromite (Simonov *et al.*, 2013) follow an olivine fractionation trend (Fig. 14), which possibly signifies that the chromian spinels were partly recrystallized during successive melting events. Phanerozoic magmas with similarly high MgO contents have been described for the Chukotat Group of Cape Smith Volcanics (Herzberg, 2004, and references therein). The parent magmas of these rocks were formed during lithosphere rifting and extension, recording a change from continental to oceanic environments.

Possible geodynamic setting

Precambrian tectono-magmatic event

Our new Neoproterozoic Os model ages along with previously determined Neoproterozoic ages (mainly Sm–Nd) from the UPB massifs attest to the involvement of ancient mantle, corresponding to the pre-Uralian history of UPB development. The nature of this Neoproterozoic event is not clear. According to Tessalina *et al.* (2007), the ultramafic complexes are Neoproterozoic ophiolites and represent relics of oceanic lithosphere developed during Timanide history, appearing to be remnants of Neoproterozoic pre-Uralian oceanic lithosphere (e.g. Samygin & Burtman, 2009). Alternatively, Puchkov (2006) suggested that the apparent Neoproterozoic ages of the Paleozoic ophiolites reflect a relict signature preserved in the mantle part of the younger ophiolites, overprinted during the process of ophiolite formation.

The Neoproterozoic signature may be also explained by the presence of ancient delaminated sub-continental lithospheric mantle (SCLM), which was incorporated in the newly formed oceanic lithosphere after the rifting of the Laurussia continent at the time of initiation of the Urals subduction-zone system, when its boundaries were considerably closer to the European (Laurussia) continental margin. This situation is common in ancient (Tessalina *et al.*, 2007) and modern (e.g. Wang *et al.*, 2003) arc systems. For example, the preservation of SCLM has been demonstrated beneath the extended margin of the Southern China block in the Taiwan Strait (Wang *et al.*, 2003). The lherzolite-bearing massifs in the Southern Urals have been previously interpreted as remnants of SCLM (Tessalina *et al.*, 2007). However, the composition of the Nizhny Tagil dunites is far more depleted compared with that of Proterozoic SCLM (Fig. 4), which is characterized by lherzolitic to harzburgitic compositions with higher CaO and Al_2O_3 contents (Fig. 4), and depletion of palladium-group PGE (PPGE: Pt, Pd, Rh) relative to iridium-group PGE (IPGE: Os, Ir, Ru, Rh) (Tessalina *et al.*, in preparation), which would make this assumption highly unlikely.

The nature of this older Neoproterozoic tectono-magmatic event, instead, may correspond to older pre-Uralian island arc development, which seems to be supported by the prominent Proterozoic Sm–Nd and Re–Os isochron ages (e.g. Ronkin *et al.*, 1997, 2009, 2012; Maegov *et al.*, 2006; Popov & Belyatsky, 2006; Tessalina *et al.*, 2007; Efimov, 2010; Petrov *et al.*, 2010) for mineral separates and whole-rocks from a number of mafic–ultramafic massifs (Table 5). Reported ages range from Mesoproterozoic (1250 ± 80 Ma; Tessalina *et al.*, 2007) to Neoproterozic (871 ± 53 Ma, Malitch *et al.*, 2011; 882 ± 83 and 804 ± 37 Ma, Tessalina *et al.*, 2007) for Ural–Alaskan-type and lherzolite-bearing massifs and Neoproterozoic–Ediacaran for Uralian–Alaskan-type massifs (Table 5; ~560 Ma; Ronkin *et al.*, 1997, 2009, 2012; Maegov *et al.*, 2006; Popov & Belyatsky, 2006; Efimov, 2010; Petrov *et al.*, 2010), the latter ages coinciding with the Timanian orogeny (Puchkov, 2010),

Table 5: Summary of Sm–Nd geochronological data for Uralian–Alaskan-type massifs in the Urals

Massif	Lithology	Sm–Nd age (Ma)	Reference
Kumba	Pl-anorthite gabbro	561 ± 28	Maegov *et al.*, 2006
Denezhkin Kamen		552–543	Efimov, 2010
Konzhakovsky Kamen	metadunites, wehrlites, clinopyroxenites, tylayites	551 ± 32	Popov & Belyatsky, 2006
Khorasyur**	Ol, Opx, Cpx, and amphibole metagabbro	565 ± 50	Ronkin *et al.*, 2009, 2012
Kytlym and Knyaspa	Ol gabbro	550 ± 25 542 ± 25	Petrov *et al.*, 2010
Yalping-Nyor	Pl, Px, Ol and WR Ol gabbro	570 ± 84	Ronkin *et al.*, 2009

WR, whole-rock.

which precedes the formation of oceanic crust in the Paleo-Uralian ocean.

Several workers (e.g. Samygin & Burtman, 2009; Samygin *et al.*, 2010) have argued about the inherited character of the Urals paleo-ocean, commencing in the Neoproterozoic with the development of an earlier pre-Uralian island arc system, based on the Neoproterozoic ages of the UPB massifs and volcanic and intrusive rocks on the western slope of the Urals, with ages ranging from *c.* 700 Ma to 515 Ma (Samigin & Rugenzev, 2003). Partial melting of these mafic–ultramafic assemblages during the reactivation of the Uralian paleo-ocean is supported by the multi-stage evolution of several Uralian mafic–ultramafic massifs based on geochronological evidence from Urals ophiolites, including (1) ages of extracted zircons (e.g. Savelieva *et al.*, 2007) and (2) Re–Os and Sm–Nd ages of several dunite–clinopyroxenite massifs (e.g. Ronkin *et al.*, 1997, 2009, 2012; Maegov *et al.*, 2006; Popov & Belyatsky, 2006; Tessalina *et al.*, 2007; Efimov, 2010; Petrov *et al.*, 2010), with younger melting events corresponding to the development of the Paleozoic Uralian paleo-ocean.

Paleomagnetic data (Petrov & Svyazhina, 2006) do not conflict with the idea that the Tagil arc was formed primarily on Vendian oceanic lithosphere of the Paleo-Asian Ocean. The present position of the arc complex at a short distance from the East European platform is connected with the activity of a Silurian–Early Devonian subduction system, dipping away from the Baltica–Laurussia continent.

The Precambrian ages may be also connected with mantle melting under the influence of either a subduction zone or a superplume, situated at a significant (thousands of kilometres) distance from the Neoproterozoic (Ediacaran) Timanide orogen. This could explain the similarity of the Uralian–Alaskan-type massifs to those occurring within stable cratons (e.g. Kondyor, Chad). The similarity of the Nizhny Tagil primary magma composition to that of Phanerozoic primary magmas from plume associations and, in particular, to the Chukotat Group volcanic series within the Cape Smith belt (Fig. 14), may signify a similar origin related to lithosphere rifting and extension during the change from a continental to an oceanic environment.

The proximity of Archean continental blocks is further supported by the preservation of Archean age zircons within the Nizhny Tagil dunites. The possibility of input and preservation of ancient zircons in mantle subsequently modified by younger mid-ocean ridge and island arc volcanism has been suggested in a number of publications (Bea *et al.*, 2001; Bortnikov *et al.*, 2005; Puchkov, 2006). However, the presence of Archean zircons in the modern intra-oceanic arcs of Vanuatu (Buys *et al.*, 2014) and the Solomon Islands (Tapster *et al.*, 2014) has been explained by the presence of remnants of older crustal fragments in the basement of the island arcs. In our case, the ages of the Archean zircons are consistent with that of the East European craton, or, more precisely, the Volga–Uralia block, adjacent to the Urals orogenic belt, which was formed as a result of a Neoarchean plume event at 2·74–2·6 Ga, transforming earlier Archean continental crust (3·4–3·0 Ga) (Mints, 2011). In the modern Urals structure, an Archean–Proterozoic sequence is present under the Southern and Middle Urals Paleozoic structures as a continuation of the East European craton. Inside the Urals structure, Archean rocks (average zircon U–Pb age of 2·9 ± 0·2 Ga) are exposed within the Taratash uplift (Puchkov, 2010).

Island arc setting

In the Urals, several workers have ascribed the formation of the UPB massifs as a whole to a suprasubduction geodynamic setting within the Silurian Tagil island arc (Ivanov & Shmelev, 1996; Ivanov *et al.*, 2007; Fershtater, 2013). The nature of the Pt-enriched signature of the zoned ultramafic–mafic massifs was previously explained by melt extraction from a sulphide-poor, Pt-enriched mantle source within a Paleozoic subduction zone, as described by Garuti *et al.* (1997) and Kepezhinskas & Defant (2001). These workers proposed a model involving multiple melt extraction events from a sub-arc mantle source, leaving refractory Pt alloys in the residual mantle. Remelting of this depleted, metasomatized and Pt-enriched mantle beneath the arc, owing to hydrous fluid fluxing from dehydrating subducted lithosphere, could potentially generate small volumes of Pt-rich primitive (picritic) liquids that fractionate in upper crustal reservoirs to form

the entire range of Uralian–Alaskan-type intrusive rocks (Kepezhinskas & Defant, 2001). Indeed, the good correlation between the PGE patterns of the Nizhny Tagil peridotites and those of sub-arc mantle in Papua New Guinea (Fig. 6; Grégoire *et al.*, 2001) seems to confirm this assumption. The trace element patterns of the dunites from the Uralian clinopyroxenite–dunite massifs are similar to those of harzburgitic mantle xenoliths from the Tabar–Lihir–Tanga–Feni arc in Papua New Guinea (Grégoire *et al.*, 2001) and display features typical of metasomatized sub-arc mantle such as LILE (Sr, Ba Rb, Th, U and Pb) enrichment (Fig. 5; Grégoire *et al.*, 2001). The negative Nb anomaly and positive anomalies at Sr and Li are typical features of suprasubduction-zone ultramafic rocks (Fershtater *et al.*, 1999). The wehrlites and clinopyroxenites associated with the dunites also show clearly pronounced suprasubduction features: negative Nb, Ti, and Zr and positive Sr anomalies (Fig. 5; Fershtater *et al.*, 1999). Redox conditions (fO_2 of 2·7 relative to FMQ; Chashchukhin *et al.*, 2014) are also consistent with an island arc setting, which is 1–4 log units more oxidized compared with MORB and ocean island basalts (OIB) (e.g. Evans, 2012). Trace element and REE data for the mafic unit show distinct LREE enrichment, which has been attributed to its island arc affinity (Sedler *et al.*, 1996). Shallow depths (*c.* 50 km) typical for sub-arc peridotites are also confirmed by calculated pressures of 18 ± 3 kbar.

However, the interpretation of the UPB dunite–clinopyroxenite–gabbro complexes as a suprasubduction-zone sequence of rocks conflicts with available geochronological data (e.g. Ronkin *et al.*, 1997, 2009, 2012; Maegov *et al.*, 2006; Popov & Belyatsky, 2006; Efimov, 2010; Petrov *et al.*, 2010), which indicate that they pre-date Urals island arc formation, and are analogous to similar rocks from platform-related massifs such as the Kondyor massif in the Aldan Shield of the Siberian Platform. These ideas were presented by Efimov (1984, 2010), who also showed that the hornfels surrounding these complexes could have a tectonic relationship with a volcanic environment. This implies that the dunites could have a distinct origin and were tectonically emplaced into the upper crust within dunite–clinopyroxenite–gabbro blocks (Efimov *et al.*, 1993).

Comparison with other zoned clinopyroxenite–dunite massifs

Uralian–Alaskan-type complexes are relatively scarce; only 46 complexes fit the definition of a dunite core surrounded by a clinopyroxenite rim (Guillou-Frottier *et al.*, 2014). Despite the very distinctive lithology, their geodynamic position varies from ancient subduction zones (Urals, Alaska, British Columbia, Kamchatka, Colombia) to intracontinental settings (Siberia, Ethiopia, Far East Russia), They were emplaced during a relatively recent period of Earth history, with ages ranging from 460 to 20 Ma (Guillou-Frottier *et al.*, 2014). However, new Os data presented in our study, together with published geochronological data for a number of UPB massifs (Ronkin *et al.*, 1997, 2009, 2012; Maegov *et al.*, 2006; Popov & Belyatsky, 2006; Efimov, 2010; Petrov *et al.*, 2010), indicate a more ancient history for the UPB massifs extending back to Neoproterozoic times.

Some of the UPB massifs, including Nizhny Tagil, contain ancient, statistically representative populations of Archean zircons, which have also been reported for dunites from the clinopyroxenite–dunite massifs of Eastern Siberia (Malitch *et al.*, 2009, 2012; authors' unpublished data). The occurrence of ancient zircons may indicate a similar geodynamic history despite their different present-day geotectonic setting, which is also expressed in the close resemblance of the platinum-bearing dunites from the Urals to those from the Aldan and Maimecha–Kotui provinces (Efimov & Tavrin, 1978; Malitch, 1999).

The Kondyor massif (Aldan Shield of the Siberian Platform) displays very similar features to the Nizhny Tagil massif, including a zoned structure, mineral chemistry, major and trace element geochemistry, PGE relative abundances, redox state and P–T–fO_2 conditions, including the temperature of olivine–chrome spinel equilibrium (Table 6; Efimov & Tavrin, 1978; Malitch, 1999; Chashukhin *et al.*, 2014). The redox conditions are very similar for the two massifs, with an oxygen fugacity of + 3·1 (log fO_2 relative to FMQ) for Kondyor, which is slightly higher than that of Nizhny Tagil (+2·7 units relative to FMQ; Chashukhin *et al.*, 2014). PGE distribution is very similar within the two massifs, with Pt/Pd ratios averaging 2·8 for dunites from Kondyor (Fig.

Table 6: Comparison between the Nizhny Tagil (Urals) and Kondyor (Aldan Shield) zoned massifs

Parameter	Nizhny Tagil	Kondyor
Lithology	dunite–(wehrlite)–clinopyroxenite	dunite-(wehrlite)–clinopyroxenite
Fo in olivine	89·8–94·5 (dunite); 87·9–88·8 (wehrlite and pyroxenite)	89·5–91 (dunite) 86–87 (wehrlite) 65–70 (clinopyroxenite)
Parental magma	subalkaline picrobasalt (Simonov *et al.*, 2013)	alkaline picrite (Simonov *et al.*, 2011)
Temperature	1345–1310°C (Cr-Sp); 1430–1360°C (Ol) (Simonov *et al.*, 2013)	1460–1300°C (Cr-Sp) 1230°C (Ol) (Simonov *et al.*, 2011)
Pressure	18 ± 2 kbar	17 ± 2 kbar
Redox (fO_2 FMQ)	2·7 (relative to FMQ) (Chashchukhin *et al.*, 2014)	3·1 (relative to FMQ) (Chashchukhin *et al.*, 2014)
La/Lu in dunite	38	1·6 (Burg *et al.*, 2009)
Pt/Pd	0·3–0·271	2·8
Tectonic setting	island arc	craton–shield (Burg *et al.*, 2009)

8). As shown in Figs 4 and 5, major and trace element variations show a close similarity for the two massifs (see also Burg *et al.*, 2009). Even more surprising is that the trace element patterns for Kondyor match very closely those of mantle xenoliths from a suprasubduction-zone setting in Papua New Guinea (Fig. 5; Grégoire *et al.*, 2001).

The processes leading to relative depletion in high field strength elements (Nb, Ta, Zr, Hf and Ti) and enrichment in LILE (Sr, Ba, Rb, Th, U and Pb) within a suprasubduction-zone setting have been identified as the product of two major processes, involving depletion by partial melting that was subsequently overprinted by oxidation and alkali enrichment related to the percolation of slab-derived, hydrous melts. These processes could account for the high oxidation state of the ultramafic rocks. These features are consistent with the long-term evolution of the platiniferous dunite and indicate a high prospectivity in noble metal mineralization within weakly eroded zoned Uralian-type massifs. These similarities together with the widespread ancient U–Pb ages of zircon in platiniferous zoned-type complexes, located within the mobile belt of the Urals and Siberian Platform, may be due to the similarity of their geodynamic evolution.

ACKNOWLEDGEMENTS

We acknowledge Professor N. McNaughton for fruitful discussions and improvement of our paper.

FUNDING

This study was partly supported by the Russian Fund for Basic Research and the Government of the Sverdlovsk Region (grant 13-05-96044-r-ural-a), the Ural Branch of the Russian Academy of Sciences (project 15-18-5-34) and the European Union through an INCO Copernicus Project (MinUrals ICA2-CT-2000-10011) and Australian Research Council through grant ARC FT110100685.

REFERENCES

Alard, O., Griffin, W. L., Pearson, N. J., Lorand, J. P. & O'Reilly, S. Y. (2002). New insights into the Re–Os systematics of subcontinental lithospheric mantle from *in-situ* analysis of sulfides. *Earth and Planetary Science Letters* **203**, 651–663.

Amossé, J. (1998). Determination of platinum-group elements and gold in geological matrices by inductively coupled plasma-mass spectrometry (ICP-MS) after separation with selenium and tellurium carriers. *Geostandards Newsletter* **22**, 93–102.

Augé, T., Genna, A., Legendre, O., Ivanov, K. S. & Volchenko, Y. A. (2005). Primary platinum mineralization in the Nizhny Tagil and Kachkanar ultramafic complexes, Urals, Russia: A genetic model for PGE concentration in chromite-rich zones. *Economic Geology* **100**, 707–732.

Bea, F., Fershtater, G. B., Montero, P., Whitehouse, M., Levin, V. Y., Scarrow, J. H., Austrheim, H. & Pushkariev, E. V. (2001). Recycling of continental crust into the mantle as revealed by Kytlym dunite zircons, Ural Mts, Russia. *Terra Nova* **13**, 407–412.

Birck, J.-L., Roy-Barman, M. & Capmas, F. (1997). Re–Os isotopic measurements at femtomole level in natural samples. *Geostandards Newsletter* **20**, 19–27.

Borg, G. & Hattori, K. (1997). Magmatic evolution of PGE-mineralization of the Nishni Tagil ultramafic complex, Urals. Biennial International Meeting. Society of Geology Applied to Mineral Deposits, Turku, Finland.

Bortnikov, P. S., Savelieva, G. N., Matukov, S. I. & Sergeev, S. A. (2005). The age of a zircon from plagiogranites and gabbro after SHRIMP data: Pleistocene intrusion in the rift valley of the Mid-Atlantic Ridge. *Doklady of Academy of Sciences* **404**, 94–99 (in Russian).

Brandon, A. D., Creaser, R. A., Shirey, S. B. & Carlson, R. W. (1996). Osmium recycling in subduction zones. *Science* **272**, 861–864.

Burg, J. P., Bodinier, J.-L., Gerya, N., Bedini, R.-M., Boudier, F., Dautria, J.-M., Prikhodko, V., Efimov, A., Pupier, E. & Balanec, J.-L. (2009). Translithospheric mantle diapirism: Geological evidence and numerical modeling of the Kondyor zoned ultramafic complex (Russian Far-East). *Journal of Petrology* **50**, 289–321.

Burton, K. W., Schiano, P., Birck, J.-L. & Allègre, C. J. (1999). Osmium isotope disequilibrium between mantle minerals in a spinel-lherzolite. *Earth and Planetary Science Letters* **172**, 311–322.

Buys, J., Spandler, C., Holm, R. J. & Richards, S. W. (2014). Remnants of ancient Australia in Vanuatu: Imlications for crustal evolution in island arcs and tectonic development of the southwest Pacific. *Geology* **42**, 939–942.

Cabri, L. J., Harris, D. C. & Weiser, T. W. (1996). Mineralogy and distribution of platinum-group minerals (PGM) placer deposits of the world. *Exploration and Mining Geology* **5**, 73–167.

Chashchukhin, I. S., Votyakov, S. L. & Pushkarev, E. V. (2014). Redox state of dunite–clinopyroxenite complexes of Ural–Alaskan-type. In: Anikina, E. V., Ariskin, A. A., Barnes, S.-J., *et al.* (eds) *12th International Platinum Symposium. Abstracts*. Institute of Geology and Geochemistry UB RAS, pp. 169–170.

Chen, J. H., Papanastassiou, D. A. & Wasserburg, G. J. (1998). Re–Os systematics in chondrites and the fractionation of the platinum-group elements in the early Solar System. *Geochimica et Cosmochimica Acta* **62**, 3379–3392.

Cohen, A. S. & Waters, F. G. (1996). Separation of osmium from geological materials by solvent extraction for analysis by thermal ionisation mass spectrometry. *Analytica Chimica Acta* **332**, 269–275.

Crocket, J. H. (1979). Platinum-group elements in mafic and ultramafic rocks: a survey. *Canadian Mineralogist* **17**, 391–402.

Danyushevsky, L. V., McNeill, A. W. & Sobolev, A. V. (2002). Experimental and petrological studies of melt inclusions in phenocrysts from mantle-derived magmas: an overview of techniques, advantages and complications. *Chemical Geology* **183**, 5–24.

Efimov, A. A. (1984). *Gabbro–ultrabasic complexes of the Urals and a problem of ophiolites*. Nauka (in Russian).

Efimov, A. A. (2010). The grand total of centennial study of the Uralian Platinum Belt. *Lithosphera* **10**(**5**), 34–53.

Efimov, A. A. & Tavrin, I. F. (1978). Common origin of platinum-bearing dunites of the Urals and Aldan Shield. *Doklady Academii Nauk SSSR* **243**, 75–77.

Efimov, A. A., Efimova, L. P. & Maegov, V. I. (1993). The tectonics of the platinum-bearing belt of the Urals: composition and mechanism of structural development. *Geotectonics* **27**, 197–207.

Evans, K. (2012). The redox budget of subduction zones. *Earth-Science Reviews* **113**, 11–32.

Fershtater, G. B. (2013). *Paleozoic intrusive magmatism of the Middle and Southern Urals*. Uralian Branch of RAS, 368 pp. (in Russian).

Fershtater, G. B., Bea, F., Pushkarev, E. V., Garuti, G., Montero, P. & Zaccarini, F. (1999). Insight into the petrogenesis of the Urals Platinum Belt: New geochemical evidence. *Geochemistry International* **37**(**4**), 302–319.

Fershtater, G. B., Krasnobaev, A. A., Bea, F., Montero, P., Levin, V. Y. & Kholodnov, V. V. (2009). Isotopic–geochemical features and age of zircons in dunites of the platinum-bearing type Uralian massifs: Petrogenetic implications. *Petrology* **17**(**5**), 503–520.

Foley, J. Y., Light, T. D., Nelson, S. W. & Harris, R. A. (1997). Mineral occurrences associated with mafic–ultramafic and related alkaline complexes in Alaska. In: Goldfarb, R. J. & Miller, L. D. (eds) *Mineral Deposits of Alaska. Economic Geology Monograph* **9**, 396–449.

Garuti, G. (2014). The chromitite–PGE association of the Urals: an overview. In: Anikina, E. V., Ariskin, A. A., Barnes, S.-J., *et al*. (eds) *12th International Platinum Symposium. Abstracts*. Institute of Geology and Geochemistry UB RAS, pp. 171–172.

Garuti, G., Fershtater, G., Bea, F., Montero, P., Pushkarev, E. V. & Zaccarini, F. (1997). Platinum-group elements as petrological indicators in mafic–ultramafic complexes of the central and southern Urals: preliminary results. *Tectonophysics* **276**, 181–194.

González-Jiménez, J., Gervilla, F., Griffin, W. L., Proenza, J. A., Augé, T., O'Reilly, S. Y. & Pearson, N. J. (2012). Os-isotope variability within sulfides from podiform chromitites. *Chemical Geology* **291**, 224–235.

Grégoire, M., McInnes, B. I. A. & O'Reilly, S. Y. (2001). Hydrous metasomatism of oceanic sub-arc mantle, Lihir, Papua New Guinea Part 2. Trace element characteristics of slab-derived fluids. *Lithos* **59**, 91–108.

Griffin, W. L., O'Reilly, S. Y., Afonso, J. C. & Begg, G. C. (2009). The composition and evolution of lithospheric mantle: a re-evaluation and its tectonic implications. *Journal of Petrology* **50**(**7**), 1185–1204.

Guillou-Frottier, L., Burov, E., Augé, T. & Gloaguen, E. (2014). Rheological conditions for emplacement of Ural–Alaskan-type ultramafic complexes. *Tectonophysics* **631**, 130–145.

Harris, D. C. & Cabri, L. J. (1991). Nomenclature of platinum-group-element alloys: review and revision. *Canadian Mineralogist* **29**, 231–237.

Hattori, K. & Hart, S. R. (1991). Osmium-isotope ratios of platinum-group minerals associated with ultramafic intrusions: Os isotopic evolution of the oceanic mantle. *Earth and Planetary Science Letters* **107**, 499–514.

Herzberg, C. (2004). Geodynamic information in peridotite petrology. *Journal of Petrology* **45**(**12**), 2507–2530.

Herzberg, C. & O'Hara, M. J. (2002). Plume-associated ultramafic magmas of Phanerozoic age. *Journal of Petrology* **43**(**10**), 1857–1883.

Ivanov, O. K. (1997). *Concentric-zonal pyroxenite–dunite massifs of the Urals (mineralogy, petrology, genesis)*. Ural State University (in Russian).

Ivanov, K. S. & Shmelev, V. R. (1996). Platinum-bearing belt of the Urals—a magmatic trace of Early Paleozoic subduction. *Doklady Earth Sciences* **347**, 649–652 (in Russian).

Ivanov, K. S., Volchenko, Yu. A. & Koroteev, M. A. (2007). The nature of the Platinum Belt of the Urals and its chromite–PGE deposits. *Doklady Earth Sciences* **417**, 1–5 (in Russian).

Kepezhinskas, P. & Defant, M. J. (2001). Nonchondritic Pt/Pd ratios in arc mantle xenoliths: Evidence for platinum enrichment in depleted island-arc mantle sources. *Geology* **29**, 851–854.

Krasnobaev, A. A. & Anfilogov, V. N. (2014). Zircons: Implications for dunite genesis. *Doklady Earth Sciences* **456**(**1**), 535–538.

Kushiro, I. (1960). Si–Al relation in clinopyroxenes from igneous rocks. *American Journal of Sciences* **258**, 548–554.

Lorand, J.-P. & Alard, O. (2001). Platinum-group element abundances in the upper mantle: new constraints from *in situ* and whole-rock analyses of Massif Central xenoliths (France). *Geochimica et Cosmochimica Acta* **65**, 2789–2806.

Maegov, V. I., Petrov, G. A., Ronkin, Yu. L. & Lepikhina, O. P. (2006). The first results of Sm–Nd isotopic dating of olivine-anorthitic gabbro of the Platinum-Bearing Belt of the Urals. In: Shardakova (ed) *Ophiolites: geology, petrology, metallogeny and geodynamics. Proceedings of International Scientific Conference (XII readings in memory of A. N. Zavaritskiy),* Ekaterinburg: Institute of Geology and Geochemistry, Uralian Branch of RAS, pp. 110–113 (in Russian).

Malitch, K. N. (1990). Peculiarities of distribution of platinum-group elements in the rocks of ultramafic massifs of the Aldan Shield. *Geochemistry International* **27**(**10**), 113–116 [translated from *Geokhimiya* 27(3), 425–429].

Malitch, K. N. (1998). Peculiarities of platinum-group elements distribution in ultramafites of clinopyroxenite–dunite massives as an indicator of their origin. In: Laverov, N. P. & Distler, V. V. (eds) *International Platinum*. Theophrastus, pp. 129–140.

Malitch, K. N. (1999). *Platinum-group elements in clinopyroxenite–dunite massifs of the Eastern Siberia (geochemistry, mineralogy, and genesis)*. St. Petersburg Cartographic Factory, VSEGEI Press (in Russian).

Malitch, K. N. & Badanina, I. Yu. (2015). Iron–platinum alloys from chromitites of the Nizhny Tagil and Kondyor clinopyroxenite–dunite massifs (Russia). *Doklady Earth Sciences* **462**(**2**), 634–637 [translated from *Doklady Akademii Nauk* **462**(6), 692–695].

Malitch, K. N., Efimov, A. A. & Ronkin, Yu. L. (2009). Archean U–Pb isotope age of zircon from dunite of the Nizhny Tagil massif (Platinum Belt of Urals). *Doklady Earth Sciences* **427**(**5**), 851–855 [translated from *Doklady Akademii Nauk* **427**(1), 101–105].

Malitch, K. N., Efimov, A. A. & Badanina, I. Yu. (2011). Contrasting platinum-group mineral assemblages from chromitites of the Nizhny Tagil and Guli massifs (Russia): implications for composition, sources and age. *Doklady Earth Sciences* **441**(**1**), 1514–1518 [translated from *Doklady Akademii Nauk* **441**(1), 83–87].

Malitch, K. N., Efimov, A. A. & Badanina, I. Yu. (2012). The age of Kondyor massif dunites (Aldan Province, Russia): First U–Pb isotopic data. *Doklady Earth Sciences* **446**(**1**), 1054–1058 [translated from *Doklady Akademii Nauk* **446**(3), 308–312].

McDonough, W. F. & & Sun, S. S. (1995). The composition of the Earth. *Chemical Geology* **120**, 223–253.

McInnes, B. I. A., McBride, J. S., Evans, N., Lambert, D. D. & Andrew, A. S. (1999). Osmium isotope constraints on ore metal recycling in subduction zones. *Science* **286**, 512–515.

Meisel, T., Reisberg, L., Moser, J., Carignan, J., Melcher, F. & Brugmann, G. (2003). Re–Os systematics of UB-N, a serpentinized peridotite reference material. *Chemical Geology* **201**, 161–179.

Melcher, F., Grum, W., Thalhammer, T. V. & Thalhammer, O. A. R. (1999). The giant chromite deposits at Kempirsai, Urals: constraints from trace element (PGE, REE) and isotope data. *Mineralium Deposita* **34**, 250–272.

Mints, M. V. (2011). 3D model of deep structure of the Early Precambrian crust in the East European Craton and paleogeodynamic implications. *Geotectonics* **45**, 267–290.

Nimis, P. (1999). Clinopyroxene geobarometry of magmatic rocks. Part 2. Structural geobarometers for basic to acid, tholeiitic and mildly alkaline magmatic systems. *Contributions to Mineralogy and Petrology* **135**, 62–74.

Nimis, P. & Ulmer, P. (1998). Clinopyroxene geobarometry of magmatic rocks. Part 1: An expanded structural geobarometer for anhydrous and hydrous, basic and ultrabasic systems. *Contributions to Mineralogy and Petrology* **133**, 314–327.

Parkinson, I. J., Hawkesworth, C. J. & Cohen, A. S. (1998). Ancient mantle in a modern arc: osmium isotopes in Izu–Bonin–Mariana forearc peridotites. *Science* **281**, 2011–2013.

Pearson, D. G., Shirey, S. B., Carlson, R. W., Boyd, F. R., Pokhilenko, N. P. & Shimizu, N. (1995). Re–Os, Sm–Nd, and Rb–Sr isotope evidence for thick Archaean lithospheric mantle beneath the Siberian craton modified by multistage metasomatism. *Geochimica et Cosmochimica Acta* **59**(**5**), 959–977.

Pearson, N. J., Alard, O., Griffin, W. L., Jackson, S. E. & O'Reilly, S. Y. (2002). *In-situ* measurement of Re–Os isotopes in mantle sulfides by laser ablation multicollector-inductively coupled plasma mass spectrometry: Analytical methods and preliminary results. *Geochimica et Cosmochimica Acta* **66**, 1037–1050.

Petrov, G. A. & Svyazhina, I. A. (2006). Correlation of the Ordovician–Devonian events at the Uralian and Scandinavian margins of Baltica: geological and paleomagnetic data. *Litosphera* **6**(**4**), 23–39 (in Russian).

Petrov, G. A., Ronkin, Yu. L., Maegov, V. I., Tristan, N. I., Maslov, A. V., Pushkarev, E. V. & Lepikhina, O. P. (2010). New data on the composition and age of complexes of foundation of the Tagil island arc. *Doklady Earth Sciences* **432**(**4**), 499–505 (in Russian).

Popov, V. S. & Belyatsky, B. V. (2006). Sm–Nd age of dunite–clinopyroxenite–tylayite association of the Kytlym massif, Platinum Belt of the Urals. *Doklady Earth Sciences* **409**(**1**), 104–109 (in Russian).

Puchkov, V. N. (2006). On the age of the Uralian ophiolites. In: Koroteev, V. A. (ed.) *Ophiolites: geology, petrology, metallogeny and geodynamics*. IG USC RAS, pp. 121–129 (in Russian).

Puchkov, V. N. (2010). *Geology of the Urals and Cis-Urals (actual problems of stratigraphy, tectonics, geodynamics and metallogeny*. Design Polygraph Service, 279 pp. (in Russian).

Reisberg, L., Lorand, J.-P. & Bedini, R. M. (2004). Reliability of Os model ages in pervasively metasomatized continental mantle lithosphere: a case study of Sidamo spinel peridotite xenoliths (East African Rift, Ethiopia). *Chemical Geology* **208**, 119–140.

Ronkin, Yu. L., Ivanov, K. S., Shmelev, V. R. & Lepikhina, O. P. (1997). On the problem of isotopic dating of the Platinum Belt of the Urals: the first Sm–Nd data. In: *Geology and raw materials of the Western Urals*. Perm State University, pp. 66–68 (in Russian).

Ronkin, Yu. L., Ivanov, K. S., Korepanov, V. B., Matukov, D. I. & Lepikhina, O. P. (2009). New data on U–Pb (SHRIMP-II) and Sm–Nd (ID-TIMS) isotope systematics of the Cis-Polar segment of the Urals. In: *Materials of the IVth Russian Conference of Isotope Geochronology 'Isotopic Systems and Time of Geological Processes'*. IGGD RAN, St. Petersburg, pp. 116–119 (in Russian).

Ronkin, Yu. L., Ivanov, K. S. & Lepikhina, O. P. (2012). Age and genetic identification of the rocks of Khorasyur massif: Sm–Nd, ID-TIMS and U–Pb SHRIMP-II restrictions. *Vestnik of the Institute of Geology Komi Science Centre*. Uralian Branch of RAS, pp. 6–10 (in Russian).

Saha, A., Basu, A. R., Jacobsen, S. B., Poreda, R. J., Yin, Q.-Z. & Yogodzinski, G. M. (2005). Slab devolatilization and Os and Pb mobility in the mantle wedge of the Kamchatka arc. *Earth and Planetary Science Letters* **236**, 182–194.

Salters, V. J. M. & Stracke, A. (2004). Composition of the depleted mantle. *Geochemistry, Geophysics, Geosystems* **5**, 1–27.

Samygin, S. G. & Burtman, V. S. (2009). Tectonics of the Urals Paleozoides in comparison with the Tien Shan. *Geotectonics* **43**, 133–151.

Samygin, S. G. & Rugenzev, S. V. (2003). The Ural Paleoocean: a model of inherited evolution. *Doklady Earth Sciences* **416**, 995–999.

Samygin, S. G., Belova, A. A., Ryazantsev, A. V. & Fedotova, A. A. (2010). Fragments of the Vendian convergent borderland in the South Urals. *Doklady Earth Sciences* **432**, 726–731.

Savelieva, G. N., Sharaskin, A. Ya., Saveliev, A. A., Spadea, P. & Gaggero, L. (1997). Ophiolites of the southern Uralides adjacent to the East European continental margin. *Tectonophysics* **276**, 117–137.

Savelieva, G. N., Suslov, P. V. & Larionov, A. N. (2007). Vendian tectono-magmatic events in mantle ophiolitic complexes of the polar Urals: U–Pb dating of zircon from chromite. *Geotectonics* **41**, 105–113.

Sedler, I., K., Borg, G., Shmelev, V., Volchenko, J., Degen, T. J., Anikina, E. & Schmidt, A. (1996). Geochemical aspects of the country rocks to the Pt-bearing zoned ultramafic complex of Nizhny Tagil, Middle Urals. *Mitteilungen der Österreichische Mineralogische Gesellschaft* **141**, 222–223.

Selby, D. & Creaser, R. A. (2003). Re–Os geochronology of organic-rich sediments: an evaluation of organic matter analysis methods. *Chemical Geology* **200**, 225–240.

Shi, R., Alard, O., Zhi, X., O'Reilly, S. Y., Pearson, N. J., Griffin, W. L., Zhang, M. & Chen, X. (2007). Multiple events in the Neo-Tethyan oceanic upper mantle: Evidence from Ru–Os–Ir alloys in the Luobusa and Dongqiao ophiolitic podiform chromitites, Tibet. *Earth and Planetary Science Letters* **261**, 33–48.

Shirey, S. B. & Walker, R. J. (1995). Carius tube digestion for low-blank rhenium–osmium analysis. *Analytical Chemistry* **34**, 2136–2141.

Shmelev, V. R. (2007). The main problems of the Urals Platinum Belt formation revisited. In: Yushkin N. P., Sazonov V. N. (Eds in-Chief), *Geodynamics, magmatism, metamorphism and mineralization*. IGG UB RAS, pp. 144–157 (in Russian).

Shmelev, V. R. & Sedler, I. (1999). The nature of the geological environment of the Urals Platinum Belt. In: Koroteev V.A. (Ed.-in-Chief), *Yearbook 1998*. IGG UB RAS, pp. 146–150 (in Russian).

Simonov, V. A., Prikhod'ko, V. S. & Kovyazin, S. V. (2011). Genesis of platiniferous massifs in the southeastern Siberian Platform. *Petrology* **19**, 549–567.

Simonov, V. A., Puchkov, V. N., Prikhodko, V. S., Stupakov, S. I. & Kotlyarov, A. V. (2013). Conditions of crystallization of dunites of the Nizhni Tagil platinum-bearing ultramafic massif (Urals). *Doklady Earth Sciences* **449**, 692–695 (in Russian).

Sluzhenikin, S. F. (2000). Low sulphide platinum mineralization in differentiated mafic–ultramafic intrusions of the Noril'sk region. Extended abstract of PhD thesis, IGEM RAS, Moscow.

Smoliar, M. I., Walker, R. J. & Morgan, J. W. (1996). Re–Os ages of group IIA, IIIA, IVA, and IVB meteorites. *Science* **271**, 1099–1102.

Sokolov, V. B. (1989). On the deep structure of massifs of the Urals Platinum Belt. *Izvestiya AN SSSR, Seriya Geologicheskaya* **11**, 73–80 (in Russian).

Tapster, S., Roberts, N. M. W., Petterson, M. G., Saunders, A. D. & Naden, J. (2014). From continent to intra-oceanic arc: Zircon xenocrysts record the crustal evolution of the Solomon island arc. *Geology* **42**, 1087–1090.

Taylor, H. P., Jr (1967). The zoned ultramafic complexes of southeastern Alaska, Part 4.II. In: Wyllie, P. J. (ed.) *Ultramafic and Related Rocks*. John Wiley, pp. 96–118.

Tessalina, S. G., Bourdon, B., Gannoun, A., Capmas, F., Birck, J.-L. & Allègre, C. J. (2007). Complex Proterozoic to Paleozoic history of the upper mantle recorded in the Urals lherzolite massifs by Re–Os and Sm–Nd systematics. *Chemical Geology* **240**, 61–84.

Walker, R. J., Horan, M. F., Morgan, J. W., Becker, H., Grossman, J. N. & Rubin, A. E. (2002). Comparative 187Re-187Os systematics of chondrites: implications regarding early solar system processes. *Geochimica et Cosmochimica Acta* **66**, 4187–4201.

Wang, K.-L., O'Reilly, S. Y., Griffin, W. L., Chung, S.-L. & Pearson, N. J. (2003). Proterozoic mantle lithosphere beneath the extended margin of the south China block: *In situ* Re–Os evidence. *Geology* **31**, 709–712.

Widom, E., Kepezhinskas, P. & Defant, M. (2003). The nature of metasomatism in the sub-arc mantle wedge; evidence from Re–Os isotopes in Kamchatka peridotite xenoliths. *Chemical Geology* **196**, 283–306.